UCLouvain

AGRO LOUVAIN

Faculté des bioingénieurs

How do root anatomy influences water uptake in tomato?

Updates of protocols and computational tools for the characterization of tomato root anatomy

Auteur : Marco D'Agostino
Promoteur : Guillaume Lobet
Lecteurs : Muriel Quinet
Valentin Couvreur

Année académique 2021-2022
Mémoire de fin d'études présenté en vue de l'obtention du diplôme de Bioingénieur : Sciences Agronomiques

Acknowledgements

D'abord, je remercie chaleureusement Valentin Couvreur et Muriel Quinet pour avoir accepté d'être lecteurs de ce mémoire. Merci pour votre temps et bonne lecture !

J'aimerais ensuite transmettre un immense merci à mon promoteur, Guillaume Lobet, qui, malgré ses innombrables activités (je le soupçonne d'avoir un retourneur de temps) était toujours disponible et ouvert à la discussion.

Merci à Rémy, compagnon de travail de ce mémoire, à qui je dois toujours deux bières pour l'avoir considéré comme un robot.

Merci à Valentin, Adrien, Thomas et Clément pour leur précieux temps et leurs minutieuses explications.

Merci à tous ceux qui, après m'avoir demandé "Tu fais sur quoi ton mémoire ?", ont eu la patience de m'écouter alors que je tentais médiocrement d'expliquer pourquoi je massacrais des racines de tomates.

Enfin, je tiens à saluer mes co-laborantins Thibauld, Hugo et Maureen, amis étudiants et mémorants tout au long de ces cinq années, sans qui je ne serais probablement jamais arrivé jusqu'ici.

Content

I. Introduction **1**

II. Context and state of the art **2**

Phenotyping 2

Root water uptake 3

Influence of the anatomy on water flow 5

II. A. 1. Primary growth 5

II. A. 2. Secondary growth in root 6

II. A. 3. Sub-cellular parameters in water flow 7

II. A. 4. Apoplastic barriers 7

Modelling anatomy and water flow 8

II. A. 5. Modelling radial water flow 8

II. A. 6. Model root anatomies 9

II. A. 7. Modelling multiscale water flow in the soil-root-system 10

Application to tomato 11

III. Objectives **12**

IV. Materials & methods **13**

Genotype selection and plant grow 13

Architectural measurements 15

Anatomical measurements 15

IV. A. 1. Samples and cross section preparation 15

IV. A. 2. Berberine aniline staining 18

IV. A. 3. Fluorol yellow staining 18

Anatomical quantifications 19

IV. A. 4. Data measurement 19

IV. A. 5. Data processing 20

Data management 21

Simulations 22

V. Results **24**

Architectural and anatomical characterization 24
V. A. 1. Architecture 24
V. A. 2. Anatomical characterization 24
V. A. 3. Quantification of the anatomy 29
GRANAR secondary growth update: Pack Xylem function 31
Water uptake 31
VI. Discussion & perspectives 34
VII. Conclusion 37
References 39
Appendices 47
Appendix 1 : Hoegland nutritive solution 47
Appendix 2 : Example of secondary growth cross sections generated with the update of GRANAR 48

List of figures

Figure 1 : RootPhAir, the aeroponic phenotyping facility of the UCLouvain 2

Figure 2 : Water flow pathways at the cross-section scale 4

Figure 3 : Anatomy of a primary growth root 5

Figure 4 : Secondary growth (left) vs. primary growth (right) in tomato 6

Figure 5 : Illustration of endodermal differentiation in Arabidopsis 7

Figure 6 : Cell-level hydraulic network 8

Figure 7 : Virtual Phenotyping Pipeline for Root Hydraulic Traits (VIPER) 10

Figure 8 : Materials for plant growth 14

Figure 9 : Cross sections were made in four segments of the main root, plus one segment for the primary stage 16

Figure 10 : Colorations used and examples of image composition 17

Figure 11 : Quantified cross-section picture 20

Figure 12 : Physical design of the database used 22

Figure 13 : Architectural results for *S. pimpinellifolium* and *S. lycopersicum* 25

Figure 14 : Apoplastic barriers along the root 27

Figure 15 : Exodermis and epidermis in segment 4 28

Figure 16 : Visualisation of anatomical quantifications. Orange is for *S. pimpinellifolium,* and green is for *S. lycopersicum* 30

Figure 17 : Comparison side by side between generated cross section and corresponding anatomy picture 32

List of tables

Table 1 : Selected genotypes 13

Table 2 : Results of analysis of the variance for leaf surface and growth rate 26

Table 3 : Summary of the features of each segment 26

Table 4 : Analysis of variance for the effect of the segment and the genotype 29

Table 5 : Parameters of the update of GRANAR. 33

List of symbols and abbreviations

BH	Berberine Hemisulfate
EPS	Expanded Polystyrene
FSPM	Functional Structural Plant Model
FY	Fluorol Yellow
k_r	Radial conductivity
K_x	Axial conductivity
RSA	Root System Architecture
UV	Ultraviolet
WEG	Water-Ethanol-Glycerol
XML	eXtended Markup Language
σ	Reflexion coefficient

I. Introduction

In a climate change and a growing population context, there is a need in innovation for stabilizing yields with sustainable methods (Hunter et al., 2017; Wheeler and von Braun, 2013). Drought incidence and severity are expected to increase in future years, inducing water stress on crops (Lobell and Gourdji, 2012; Tebaldi and Lobell, 2008). Identifying and adopting drought resistant cultivars through plant breeding could therefore have a significant impact on global food security. To find cultivars adapted to water stress conditions, we need to 1) identify the traits that play a role in the water uptake and drought adaptation, 2) quantify these traits and study the distribution of the quantifications among genotypes of the plant of interest, and 3) select the adapted genotype or move to genetic analysis. While phenotyping and plant breeding excel at the last two points, there is still research to perform in the first point to fully understand the implication and the behaviour of traits in plant water dynamics.

As roots plays a key role in plant growth and development since it is the place of water and nutrients extraction from the soil, root traits based phenotyping platforms have flourished. Root system architecture is a well-studied domain and is massively targeted by phenotyping processes (Atkinson et al., 2019; Wasaya et al., 2018). On the lower scale, anatomy of roots influence nutrient uptake, and anatomical phenes are attractive targets for the development of efficient and resilient crops (Lynch et al., 2021, 2014). Understanding the most influent anatomical traits and their role in water uptake is therefore crucial for introducing anatomy-based phenotyping, which, coupled with current phenotyping techniques, might help to find trait combinations that improve water uptake.

Since studying the direct influence of specific traits on water dynamics is experimentally difficult, computational tools can help simulate the impact of specific traits at low cost and have a huge potential in identify combinations of traits that optimize water uptake. Heymans et al. (2021, 2020a, 2020b) have developed a modeling pipeline that simulates water flow in monocots. They studied the impact of anatomical traits and investigated combinations of architectural and anatomical traits that are the most adapted in specific environments.

In this work, I continue and extend the work of Heymans et al. (2021, 2020a, 2020b) by modifying the modeling pipeline to dicotyledons. More specifically, I used tomato as a dicotyledon model, and I studied the impact of specific tomato anatomical traits on water uptake. For that, I developed a methodology to 1) characterize and quantify wild (*Solanum pimpinellifolium*) and domestic tomato (*Solanum lycopersicum*) root anatomy, 2) adapt a computational tool to generate corresponding anatomies, and 3) model and compute the water flow through these anatomies.

II. Context and state of the art

Phenotyping

While genotype refers to the expression of the genetic material of an individual (or in our case the shared genetic material of a species), phenotype is the set of observable traits of this individual. Phenotype is thus the result of the interaction between genotype and environmental factors. To select the best adapted plant in a set of genotypes to a given situation (in our case water stress resistance), plant breeders need quantification of the phenotype of these plants.

Phenotyping is defined as a set of methods that aims to quantify specific traits of plants (Ghanem et al., 2015). A plant trait, or phene, refers to a morphological, physiological or phenological feature. For root architecture, image-based phenotyping is broadly applied since it is non-destructive (Wasaya et al., 2018). As roots in soil are tricky to quantify accurately, soil-free methods like hydroponics, aeroponics, rhyzotrons or pouches has been widely used, and new technologies are being actively developed (Atkinson et al., 2019). High-throughput phenotyping platforms have been engineered for roots (Yang et al., 2020), like RootPhAir (Draye et al., 2018) here at the UCLouvain. At the same time, efficient image analysis tools have been developed and recognized, such as SmartRoot (Lobet et al., 2011), RootNav (Pound et al., 2013) or DIRT (Das et al., 2015).

Figure 1 : RootPhAir, the aeroponic phenotyping facility of the UCLouvain. Pictures from Draye et al. (2018)

While root architecture defines the global water flow dynamics at the plant scale, root anatomy influences local water uptake. Combining anatomy and architecture is thus necessary to fully understand water dynamics in plants. Nevertheless, at the cross-section scale, high-throughput phenotyping of root anatomy still must be developed. Analysing anatomy is time consuming. Generating large amount of anatomical data like root architecture phenotyping do is laborious, although new technologies make progress in the domain, like laser ablation

tomography (Strock et al., 2019) or X-ray microscopy (Duncan et al., 2022).

As phenotyping becomes increasingly fast, accurate and affordable, the need in understanding the behaviour and the implication of measured traits in water uptake still stands. Moreover, traits conferring drought resistance can present dual effects in function of the drying scenario, adding complexity to the selection of traits of interest (Tardieu et al., 2017).

Root water uptake

Accurately measuring water flow in plants is a limiting step in the study of soil-plant water relations (Passot et al., 2019). Pressure probe is used to measure axial and radial conductivities at the cell and the organ scale but it is costly and time-consuming (Steudle et al., 1987). Instead, functional-structural plant models (FSPM) can be used. FSPM are constituted of a detailed root system architecture (RSA) representation and functional properties. Structural information can be provided by virtual RSA, with root system simulators like RootTyp (Pagès et al., 2004), ArchiSimple (Pagès et al., 2014) or CRootBox (Schnepf et al., 2017). Functional properties are tricky to obtain experimentally but can be found in the literature. With FSPM, water flow can therefore be modelled using mathematical equations that describe known physical processes.

Water movement in plants is driven by a difference in water potential through the whole plant, between the soil and the leaves. Water evaporation through stomata at the leaves creates a tension that is sufficient to pump water from the soil, thanks to the highly cohesive power of water. This cohesion-tension theory proposed almost 130 years ago, although well discussed and criticized, still is the main theory to explain water dynamics in plants (Steudle, 2001a). This water movement from soil to leaves can be expressed as a combination of a radial flow from the soil to the xylem vessels and an axial flow through the xylem files. The axial flow J_x $[m^3 s^{-1}]$ through xylem is represented by:

$$J_x = K_x \frac{\Delta\psi}{\Delta x} \quad (1)$$

were K_x $[m^4\ s^{-1}\ MPa^{-1}]$ is the axial conductance in xylem, and $\frac{\Delta\psi}{\Delta x}$ $[MPa\ m^{-1}]$ is the gradient of water potential along the vertical length of the xylem vessel. K_x can be found using the Hagen-Poiseuille equation:

$$K_x = \sum_{i=1}^{N} \frac{\pi r_i^4}{8\eta} \quad (2)$$

where N is the number of xylem vessels, r_i is the radius of the i^{th} xylem file, and η is the water dynamic viscosity (Lewis and Boose, 1995; Steudle and Peterson, 1998).

For the radial flow in roots, the composite transport model proposes two parallel pathways for the passage of water from the soil to the xylem (Kim et al., 2018; Steudle, 2001b) : the cell-to-cell path and the apoplastic path. Cell-to-cell path consists of passing water through membranes (trans-cellular path, by diffusion or with aquaporins) or through plasmodesmata and cytosols (symplast). These pathways have different "selectivity" that is expressed by the reflexion coefficient σ. σ is close to zero for the apoplastic pathway, which does not select water and solutes, and is close to one for symplastic pathway, due to aquaporins that create the semi-permeability of the cell membranes (Couvreur et al., 2018; Kim et al., 2018).

The water flow J_w $[m^3 s^{-1}]$ at the root surface can therefore be represented:

$$J_w = 2\pi r h * k_r * \left(\Delta\psi_p + \sigma_r \, \Delta\psi_o\right) \quad (3)$$

where $2\pi r h$ $[m^2]$ is the root surface (with r the radius of the root and h the height of the cross-section), k_r $[m^3 m^{-2} s^{-1} MPa^{-1}]$ is the root radial conductivity (expressed here per surface area), $\Delta\psi_p [MPa]$ is the difference in water pressure potential between the root surface and the xylem, and $\Delta\psi_o [MPa]$ is the difference in osmotic potential between the root surface and at the xylem (Couvreur et al., 2018). However, this equation is dependent of the nature of k_r, which can be difficult to model. At the cell scale, the radial conductivity depends on the conductance of cell membranes, plasmodesmata and aquaporins (see Section II. A. 3). At the cross-section scale, anatomy (tissue types and patterns) and apoplastic barriers modify the water dynamics. These two topics are explored in the next sections.

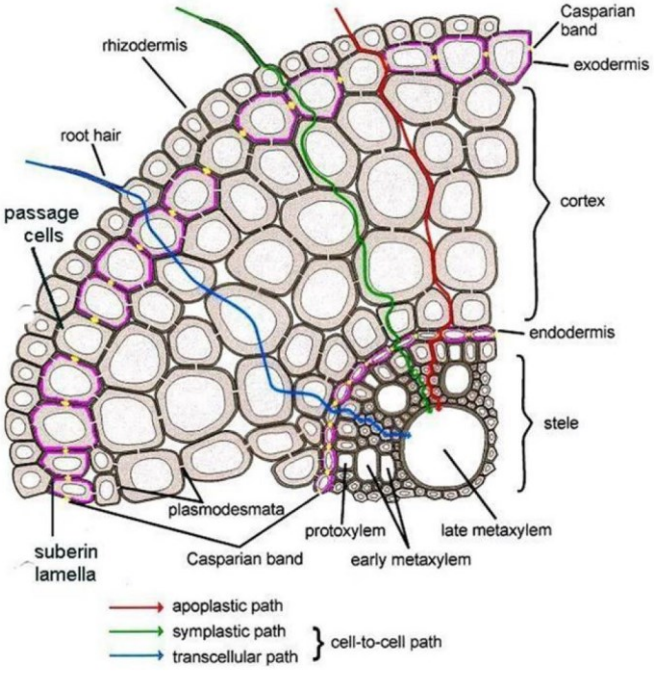

Figure 2 : Water flow pathways at the cross-section scale. Image from Kim et al. (2018).

At the plant scale, K_x and k_r can be combined within a root architecture to find a root system conductivity and therefore model the water dynamics in given soil and weather conditions (Meunier et al., 2020, 2017).

Influence of the anatomy on water flow

II. A. 1. Primary growth

In tomato, the root cross section is composed of the stele and the cortex. In a young root in primary growth, the centre of the stele is occupied by xylem and metaxylem vessels arranged around parenchyma cells. Xylem is a conductor tissue consisting of dead cells that let water and minerals flows from the root to the shoot with little resistance (Taiz and Zeiger, 2003). In primary growth, xylem forms archs, organised in blades. **Figure 3** shows 4 xylem blades but note that tomato presents a 2-blades organised xylem (see **Figure 4**). With age, xylem differentiates into metaxylem, characterised by large cells with a lignified wall, and lose its arch structure for a more random distribution around the centre. Between xylem vessels, parenchyma cells fill the rest of the inner stele. The inner stele is surrounded by phloem and pericycle layers. Phloem is the second vascular element of the root and is responsible for the transport of metabolites from the shoot to the root. Pericycle is the outer layer of the stele and is an internal meristematic tissue. It is the place of birth of lateral and adventitious roots.

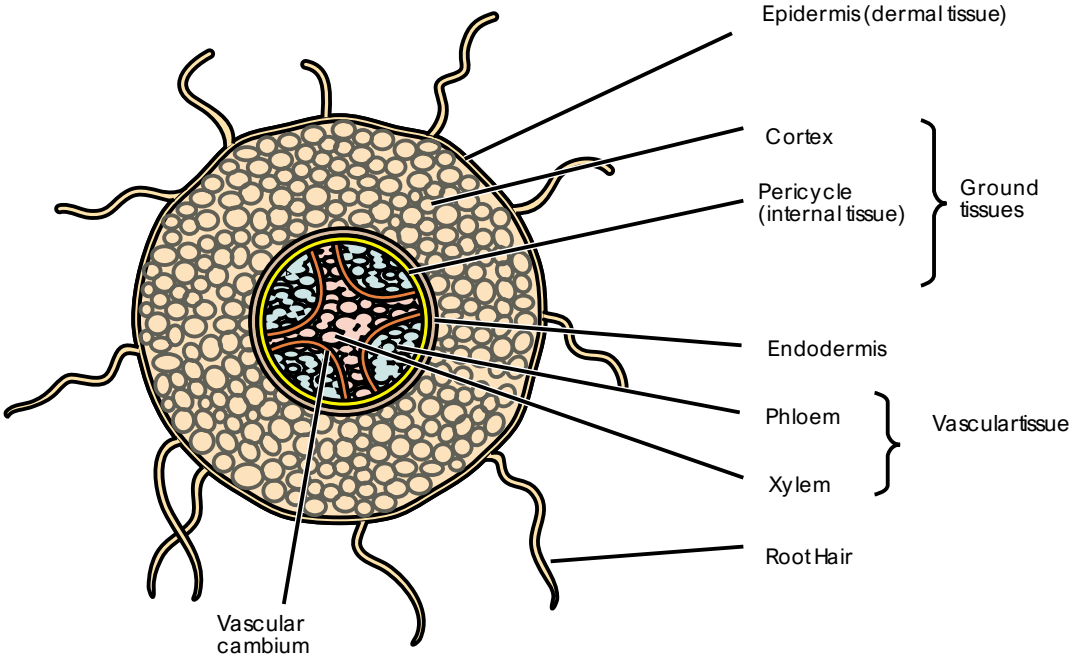

Figure 3 : Anatomy of a primary growth root. Image from Taiz & Zeiger (2003).

The cortex is composed of unspecialised cells, except for the innermost and outermost layers. The innermost layer, close to the pericycle, is the endodermis, a tissue that will usually present apoplastic barriers like Casparian strips and suberin lamellae to force symplastic pathway (see section II. A. 4). The outermost layer of the cortical cylinder is the exodermis, which will present the same apoplastic barriers that the endodermis, although the maturation timing is different.

Eventually, the epidermis is a layer at the outside of the cortex, derived from the protoderm, and that acts as a protective physical barrier.

As said before, the axial water flow in roots K_x is only dependent on the size of xylem vessels. Regarding the implication of each tissue in radial water flow, the width of the cortical layers appears to be an important factor (Chimungu et al., 2014) and one of the major predictors of k_r in maize (Heymans et al., 2020a). So far, the importance of the cortical layer width in constraining k_r of tomato roots remains unexplored.

II. A. 2. Secondary growth in root

While primary growth is the constitution of the different tissues in the root, secondary growth consists of the enlargement of the radius, where the vascular cambium divides periclinally into secondary metaxylem or parenchyma in the inside, and secondary phloem in the outside (see **Figure 4**). The stele will therefore grow, putting pressure on the cortical cylinder. In some plants, the pericycle of old roots in secondary growth differentiates into a protective tissue called periderm, which will replace the epidermis. However, in tomato no clear periderm is formed (Arafa, 2015).

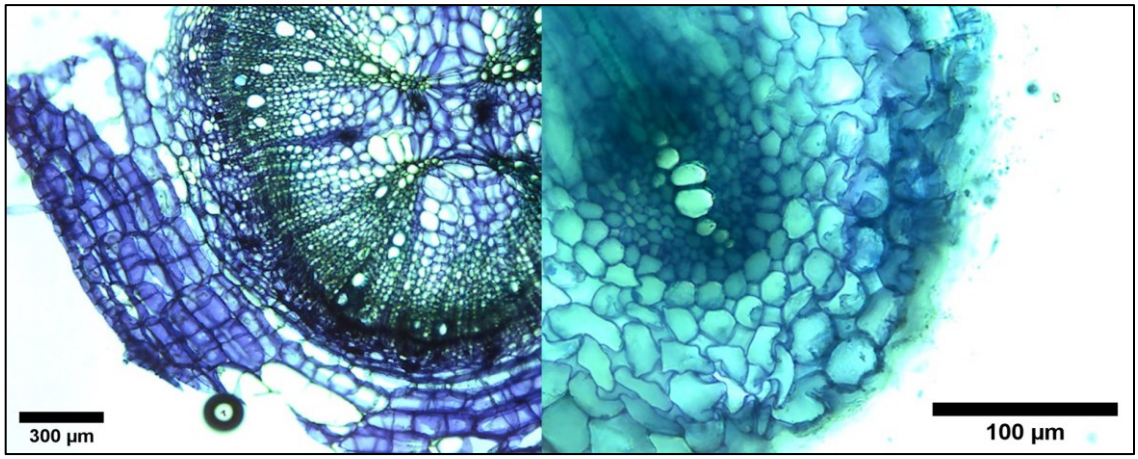

Figure 4 : Secondary growth (left) vs. primary growth (right) in tomato.

Secondary growth patterns in root anatomy play a major role in soil resource acquisition and plant fitness under stress by adding protective layers (Strock et al., 2018; Strock and Lynch, 2020), and secondary growth regulation and initiation are actively investigated (e.g., Miyashima et al., 2019; Smetana et al., 2019). From a water uptake perspective, the common sense would be to assume that secondary growth structures coupled with high-suberised tissues block the radial water flow (Steudle, 2001b). However, Gambetta et al. (2013) showed that suberised roots with secondary growth patterns can contribute significantly to the root system water uptake since they represent a great proportion of the total root area, even with a much smaller hydraulic conductivity. In tomato, the fact that no clear periderm is

formed motivates the interest for studying the impact of secondary growth structures on water flow.

II. A. 3. Sub-cellular parameters in water flow

At the cell scale, the water flow is regulated by aquaporins and plasmodesmata. Because we will use these terms in future sections, we need to briefly define them. Aquaporins are small membrane proteins that control the transcellular water movement. They therefore regulate the cell membrane permeability, and their expression varies with species and local conditions (Chaumont and Tyerman, 2014). On the other hand, plasmodesmata are channels between two cells, that traverse cell walls. They are formed during mitosis and are composed of one desmotubule that links the endoplasmic reticulum of two neighbouring cells. Plasmodesmata are important for the passage of information molecules, and regulates the symplastic water pathway (Maule, 2008).

II. A. 4. Apoplastic barriers

In roots, formations of lignin and suberin play a major role in water and ions flux regulation. Suberin is an insoluble poly(acylglycerol) polyester and forms lamellae in cell walls that serve as protection against biotic and abiotic stresses (Serra and Geldner, 2022). Lignin is a hydrophobic polymer that is found in cell walls, and that, in combination with hydrophilic components such as cellulose,

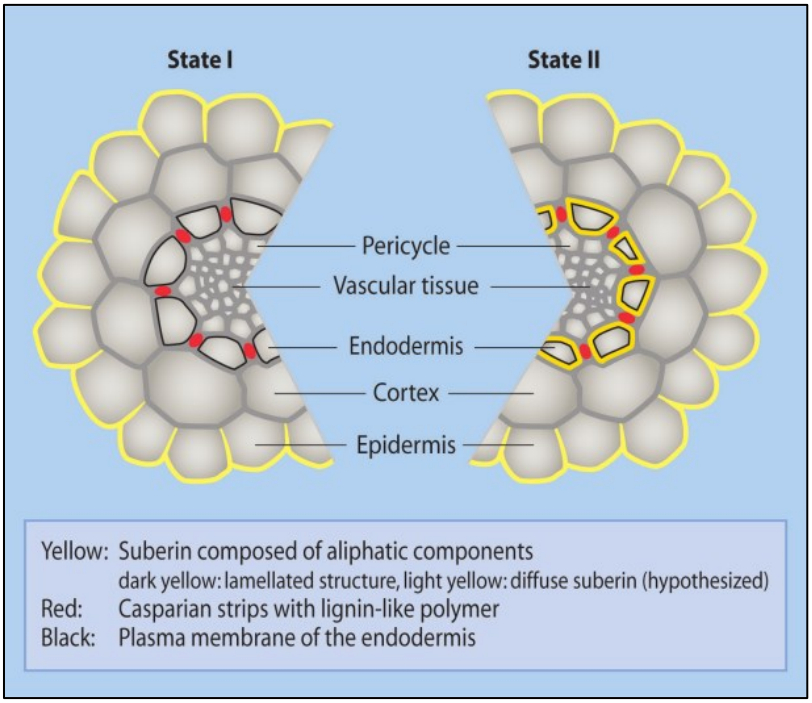

Figure 5 : Illustration of endodermal differentiation in Arabidopsis. Picture from Nawrath et al. (2013).

hemicellulose and pectin, provides strength to the cells and allows an efficient water conductivity.

Both endodermis and exodermis present maturation stages composed of Casparian strips or suberin lamellae. In the endodermis, Casparian strips are ringlike incrustations of lignin and in less proportion suberin into cell walls (Nawrath et al., 2013). Casparian strips are thought to be essential since they are consistently found in plants (Naseer et al., 2012). The two main functions of Casparian bands are 1) prevent apoplastic passage of ions from the cortex to the stele, and 2) prevent backflow of the apoplast of the stele to the apoplast of the cortex (Enstone et al., 2002). After the formation of Casparian bands, a suberin lamellae can be formed as secondary walls of the endodermis. Its main function is to prevent ions in the apoplast from penetrating endodermal cells (Enstone et al., 2002). In exodermis, Casparian bands and suberin lamellae can be observed, but in a closer timing: suberin lamellae develops during or immediately after Casparian strips. Since Casparian strips and suberin lamellae blocks water flow in apoplastic and symplastic way, respectively, they therefore have a huge impact on the radial conductivity of the root.

Modelling anatomy and water flow

II. A. 5. Modelling radial water flow

The radial conductivity k_r of a cross section depends on the global layout of tissues and apoplastic barriers. To compute the water flow at the cross-section scale, Couvreur et al. (2018) developed MECHA, a two-dimensional transverse model. MECHA computes the water flow through the cells by combining local and subcellular parameters such as plasmodesmata, aquaporins and cell wall conductivities. MECHA uses vectorised and labelled cross sections as an eXtended Markup Language (XML) file. Subcellular hydraulic data was found in the literature. MARSHAL combined the cross-section geometry and subcellular conductivities to compute water flow between cells, based on the idea that the cross section is a hydraulic network of resistances and that Ohm's law and Kirchhoff's law apply for the passage of water (**Figure 6**). The radial

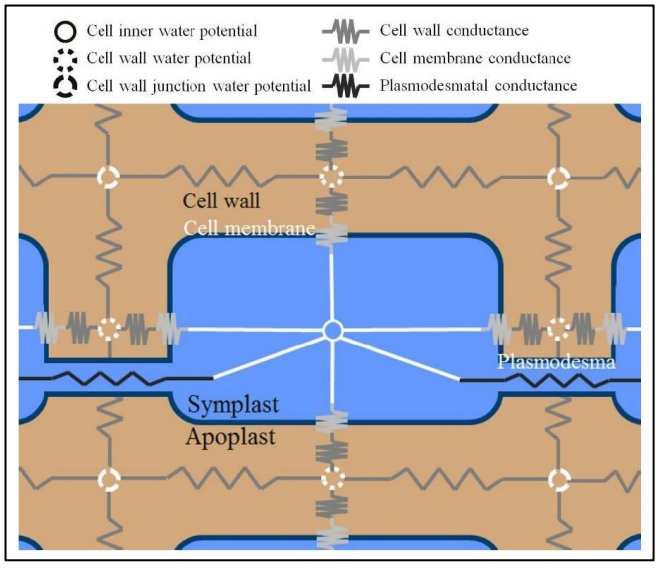

Figure 6 : Cell-level hydraulic network. Supplemental figure of Couvreur et al. (2018).

conductivity k_r is then calculated based on Equation 3 and defined as a water uptake rate per root surface under a pressure difference between root surface and xylem.

II. A. 6. Model root anatomies

While MECHA is easy to run and provide good results for a given cross section, getting such labialised cross-section is quite difficult and was the main issue for large scale, high-throughput analysis of the influence of specific anatomical traits on water uptake (Passot et al., 2019). Cross-section pictures needed to be fully labelled with CellSet (Pound et al., 2012) in order to get the XML file, which is highly time consuming.

To tackle this gap, Heymans et al. (2020a) implemented GRANAR, a generator of root anatomy. GRANAR is a set of R functions that allows the generation of XML vectorised root cross sections with simple inputs that can be easily measured on cross section pictures, e.g. by manual quantifications with ImageJ (Schneider et al., 2012) or with automated tools like RootScan (Burton et al., 2012). The generation of anatomy in GRANAR consists of placing cell layers around the centre of the root. The position and the size of a cell or cell layers depend on the cell type and on a random factor that brings slight changes at each iteration of a same set of parameters. First, the model set up a network of coordinates corresponding to the centre of each cell. The process begins by placing parenchyma cells in the stele, and then build the other tissues until the outermost layer (the epidermis) is finished. Regarding the vascular structures, the generation differs for monocotyledons and dicotyledons. In monocots, xylem poles are disposed at the periphery of the stele. On the other hand, vascular blades of xylem are formed in dicots. The number of blades and the maximum size of xylem files are input parameters, and GRANAR generates vascular blades by placing the largest xylem cell on the centre while filling the blades with decreasing cell size, until the last xylem cell of the blade have the size of a parenchyma cell. For phloem generation, GRANAR set up phloem poles between xylem blades. Pericycle, endodermis, cortex, exodermis, and epidermis layers are created by placing the centre of each cell in respect for mean cell sizes in input. Once the centre of each cell is set up, GRANAR build the cell walls using a Voronoi tessellation. Eventually, a polygon function computes the area of the cells. Since GRANAR was initially built for maize, the generation of dicotyledonous cross sections is more illustrative than functional, and was based on Arabidopsis (*Arabidopsis thaliana)*, which is a simple plant in terms of root anatomy. In the case of tomato, the first version of GRANAR can be used to generate very young roots where vascular blades are distinct (see **Figure 17.A**). Nevertheless, the anatomy of tomato roots rapidly changes after a few centimetres from the tip, and secondary growth structures appear (e.g., the replacement of xylem blades by a random distribution of xylem files, a whole cell layer of phloem and cambium), which cannot be simulated with GRANAR.

For maize, GRANAR and MECHA were coupled to study the influence of main anatomical traits on root radial conductivity, and the results highlighted the importance of cortex cells width and stele area (Heymans et al., 2020a). At the root system scale, Heymans et al. (2021) built hydraulic atlases by generating anatomies along the roots and computing water flow in these cross sections. Anatomies were generated based on microscopical measurements, while water flow was computed with MECHA for radial conductivity and the Hagen-Poiseuille equation for the axial conductivity.

This allowed the study of the behaviour of the conductivities through the root system, and comparisons with experimental measures from the literature, e.g. with the work of Doussan (1998).

II. A. 7. Modelling multiscale water flow in the soil-root-system

Then was built VIPER, the Virtual Phenotyping Pipeline for Root Water Uptake (Heymans et al., 2020b). VIPER coupled local water dynamic modelling of GRANAR-MECHA with a virtual plant architecture simulated with CRootBox (Schnepf et al., 2017) or CPlantBox (Zhou et al., 2020). Then MARSHAL (Meunier et al., 2020) coupled with Hydrus-1D (Šimůnek et al., 2016) computed the global root system conductance K_{rs}, the standard sink fraction SSF and the transpiration allowed by the root system in given soil and weather conditions.

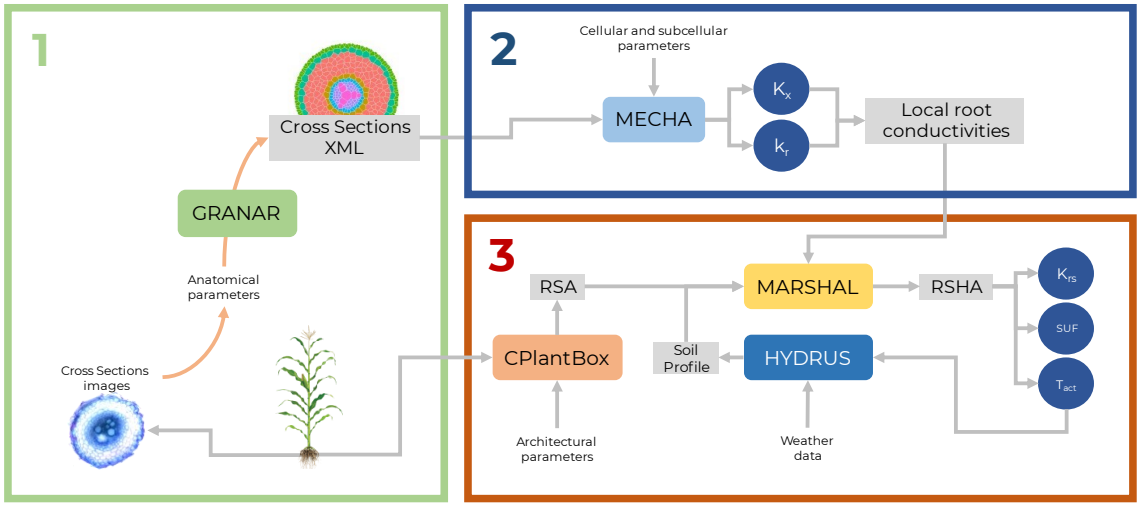

Figure 7 : Virtual Phenotyping Pipeline for Root Hydraulic Traits (VIPER).

Application to tomato

Tomato was chosen here as model plant to elaborate and calibrate modelling tools that could be applied to dicotyledons. Tomato is easy to grow in greenhouses, present secondary growth patterns while being herbaceous. Furthermore, tomato is well studied in the laboratory so I could benefit from experimental knowledge and experience (e.g. Bigot et al., 2022; Blanchard-Gros et al., 2021; Gharbi et al., 2018).

Domestic tomato (*Solanum lycopersicum*) is one of the most important vegetable crops in terms of production (FAO, 2022). However, domestic tomatoes have a very poor genetic diversity, where wild tomato genetic diversity is huge (Rezk et al., 2021). Transferring wild tomatoes benefits to domestic cultivars is subject to lots of work and application of brand new genetic techniques (Al-Khayri et al., 2021; Li et al., 2018).

Studying influent parameters in wild tomato and compare it with domestic tomato is therefore a key step before high-throughput phenotyping and elaborating breeding programs. We choose to work here with *Solanum pimpinellifolium* which is a wild but genetically close relative of *S. lycopersicum* (Bedinger et al., 2011). *S. pimpinellifolium* presents interesting genetic and geographical distributions among its 269 accessions, is resistant to salinity, and presents various architectural ideotypes (Conesa et al., 2017; Li et al., 2018; Lin et al., 2020; Chandrasekhar and Julkowska, 2022; Razali et al., 2018). These features make *S. pimpinellifolium* a good model plant to study the distribution of architectural and anatomical trait quantifications among its accessions. *Solanum lycopersicum* Moneymaker was chosen as domestic species, since it is very popular and widely used for crop production (e.g. Lee, 2021; “Moneymaker,” 2022; “Tomato ‘Moneymaker’ seeds,” 2022) .

III. Objectives

This master's thesis focusses on the following question :
"***How do anatomical root traits influence water uptake in tomato?"***

More precisely, we will focus on the influence of young secondary grow features, anatomical patterns and apoplastic barriers on hydraulic conductivities in wild and domestic tomatoes. Formally, the objectives are:

1) **Characterise and quantify tomato root anatomy.** For that, wild and domestic tomatoes will be grown. Root cross sections will be prepared and observed with a microscope. Anatomy pictures will be analysed and quantified.
2) **Adapt GRANAR** (Heymans et al., 2020a) **to generate corresponding anatomies.** Coding and calibrating new implementations of GRANAR will be done in collaboration with Rémy Schoppach[1].
3) **Compute water flow through generated anatomies.** Simulations with MECHA (Couvreur et al., 2018) will be performed on generated anatomies. Influence of anatomical traits and difference between wild and domestic tomato will be analysed. Unfortunately, this third goal will not be achieved in this master's thesis, due to a lack of time.

Eventually, this work can be seen as a protocol improvement that can be later applied to larger set of samples. This protocol prepares the basis for a more complete and complex modelling pipeline similar to VIPER (Heymans et al., 2020b) for studying global hydraulic dynamics in dicotyledons in response to different anatomical, architectural and environmental parameters.

[1] ELIA, UCLouvain.

IV. Materials & methods

Genotype selection and plant grow

Six genotypes of *Solanum pimpinellifolium* were selected based on unpublished data from Clément Sain-Cast[2] and on data from Chandrasekhar and Julkowska (2022) on weight of aerial parts, stem diameter, stem length, leaf area, root diameter and root length. From 20 genotypes at our disposal, we chose 6 genotypes by trying to maximise the contrast of the previous measurements, shown in **Table 1**. The "Population" column refers to the geographical location of the genotypes, in the populations defined by Lin et al. (2020) and data from the Tomato Genetic Research Center[3].

Table 1 : Selected genotypes

Identifier	Species	Assession	Population
A	*Solanum pimpinellifolium*	LA0114	Central
B	*Solanum pimpinellifolium*	LA0391	Central
C	*Solanum pimpinellifolium*	LA1332	Southern
D	*Solanum pimpinellifolium*	LA1599	Central-south
E	*Solanum pimpinellifolium*	LA1652	Southern
F	*Solanum pimpinellifolium*	LA1687	Central-North
G	*Solanum lycopersicum*	Moneymaker	-

A hydroponic system was designed. Web-tubes were constructed with 2cm^2 surface plastic web stuck between two PVC tubes. The web-tubes were fixed into holes made in expanded polystyrene (EPS) plates. 2,5L plastic boxes were filled with Hoagland nutrient solution (see Appendix 1 : Hoegland nutritive solution), and the EPS plates with the web-tubes were put on top of the boxes to float on the solution.

[2] EGFV, INRAE
[3] https://tgrc.ucdavis.edu/

Seeds were dropped into the web-tubes and each box went to germination chamber at 20°C, 14h/24 light for 14 days, till having 3-4 cm long root. After 14 days, the small plants were carefully removed from the web-tubes and the web-tubes were detached from the EPS plates. The young plants were fixed at the EPS plates by sticking the collar at the plate with wadding. Eventually, the plates were deposited on the solution in the bins, with the roots emerged into the solution. Then plants were grown in greenhouses for 15 days. Nutrient solution was renewed every week.

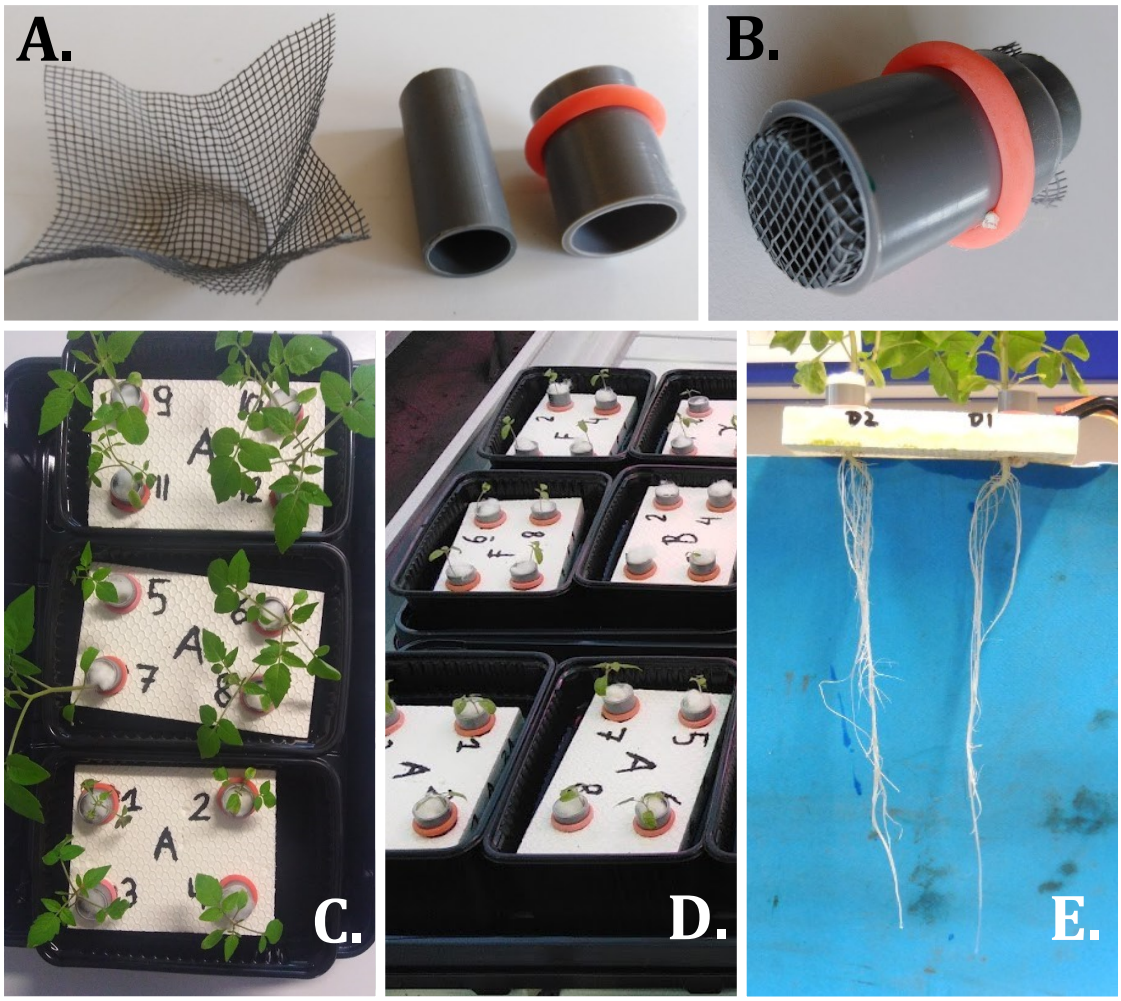

Figure 8 : Materials for plant growth. **A.** and **B.** Web-tubes composed of one plastic web and two PVC tubes. **C.** and **D.** Hydroponic system for plant growth. **E.** Capture of the root architecture 25 days after germination.

Architectural measurements

During the growth period, pictures of the root system were taken at four different dates. At each date, the plates were suspended outside of the solution, and the root systems were photographed. Architectural measures were made using SmartRoot (Lobet et al., 2011). The plants were harvested 31 days after germination. For each plant, the root system was separated from the shoot at the collar. The leaf area was measured with the Li-3100 Area Meter from LI-COR. The root system was scanned with at 600dpi resolution, then stored in tubes in a 3:3:2 water-ethanol-glycerol solution (WEG) at 2°C. WEG is a safe alternative to the well-known ethanol-acetic acid-formaldehyde (FAA) which is very toxic, and provide full integrity preservation (Kitin et al., 2020).

Anatomical measurements

IV. A. 1. Samples and cross section preparation

For each plant, the main root was pruned from its lateral roots. Inspired by Gambetta et al. (2013), the main root was divided in four segments, as distance reference from the collar (**Figure 9**). That choice was motivated by the fact that precisely measure the distance of a cross section to the apex is laborious, while working with zones and interpolate measures is simple. Furthermore, that allowed us to make large number of cross sections and select the best for each segment. The length of each segment was defined based on test observations so that each segment roughly corresponds to a homogenous anatomical pattern. The first segment is 1,5 cm long starting from the collar (~10-15 cm from the tip) and corresponds to the transition of root into shoot. Secondary growth is visible, and vascular bundles begin to form. The second segment is 2 cm long and corresponds to the fulfilment of secondary growth, at 2 cm from the collar (~8-10 cm) from the tip. Xylem files seems to follow a purely random distribution in the stele (although we sometimes see medullary rays) and the cortical cylinder is squeezed by the stele. The third segment is 2-3 cm long, corresponding to the beginning of secondary growth (at ~6-8 cm from the tip). Finally, the fourth segment is ~4 cm long, corresponding to the maturation of the primary stage of the root (at ~2-6 cm from the tip), and presenting approximately the same anatomical patterns in a large part of the root. In addition to these four segments, a last segment corresponds to the meristematic zone, from the tip up to ~1-3 cm. We did not take this segment into account in this work since it was very laborious to get such cross sections and that too few cross-section images produced within this zone were of the minimum quality required to allow a fair quantification of tissues sizes.

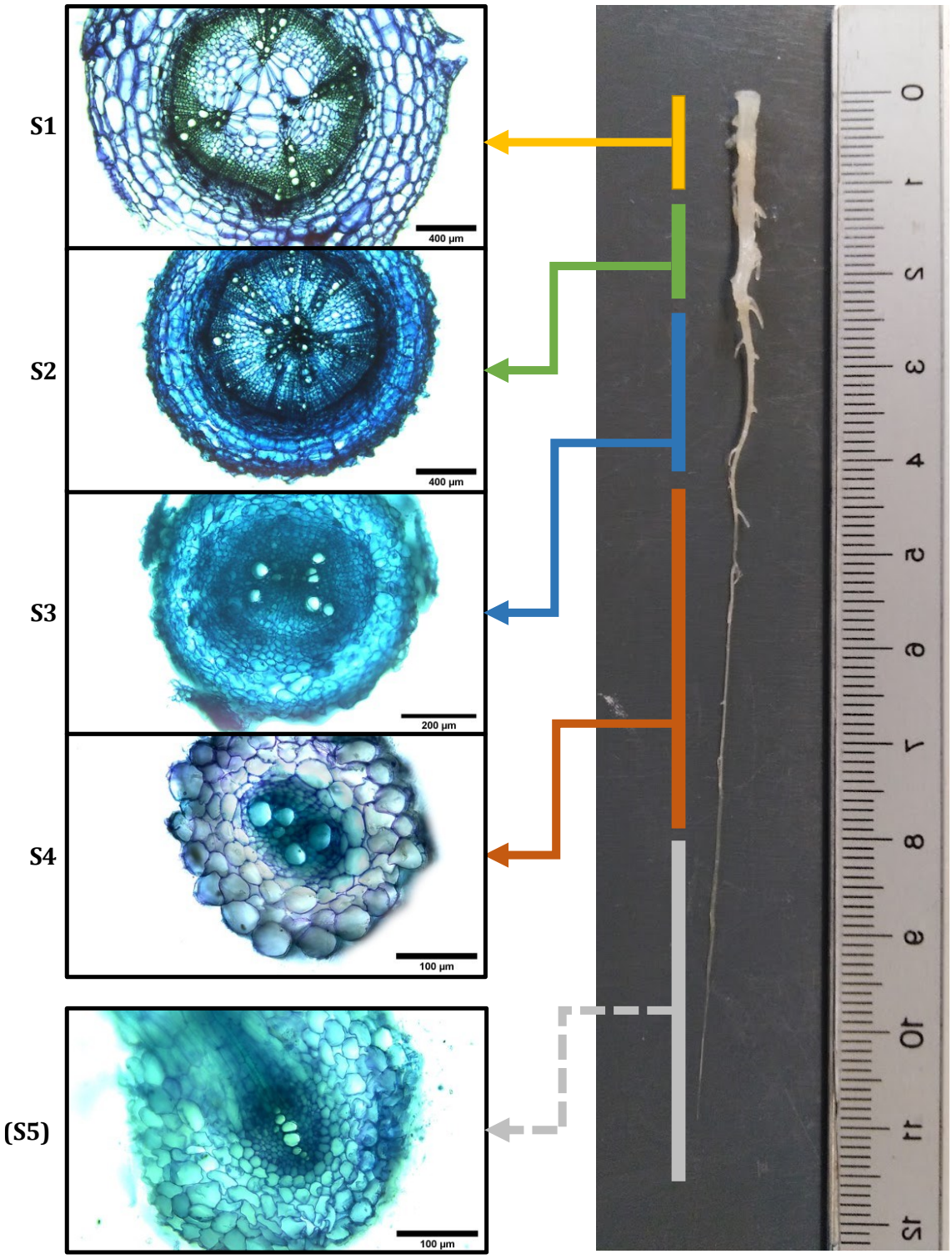

Figure 9 : Cross sections were made in four segments of the main root, plus one segment for the primary stage.

Cross sections were directly made by hand for the two first segments, while the third and the fourth segment were first embedded in agarose, following the Atkinson and Wells (2017) and Zelko et al. (2012) protocol. In our case, the protocol consists of placing the root samples in 3D printed moults from Atkinson and Wells (2017) models, and preparing an agar-water solution 5 % (w/v) at 90 °C. The agar solution was then carefully cast into the moults, which were next stored for 10 min at 2°C.

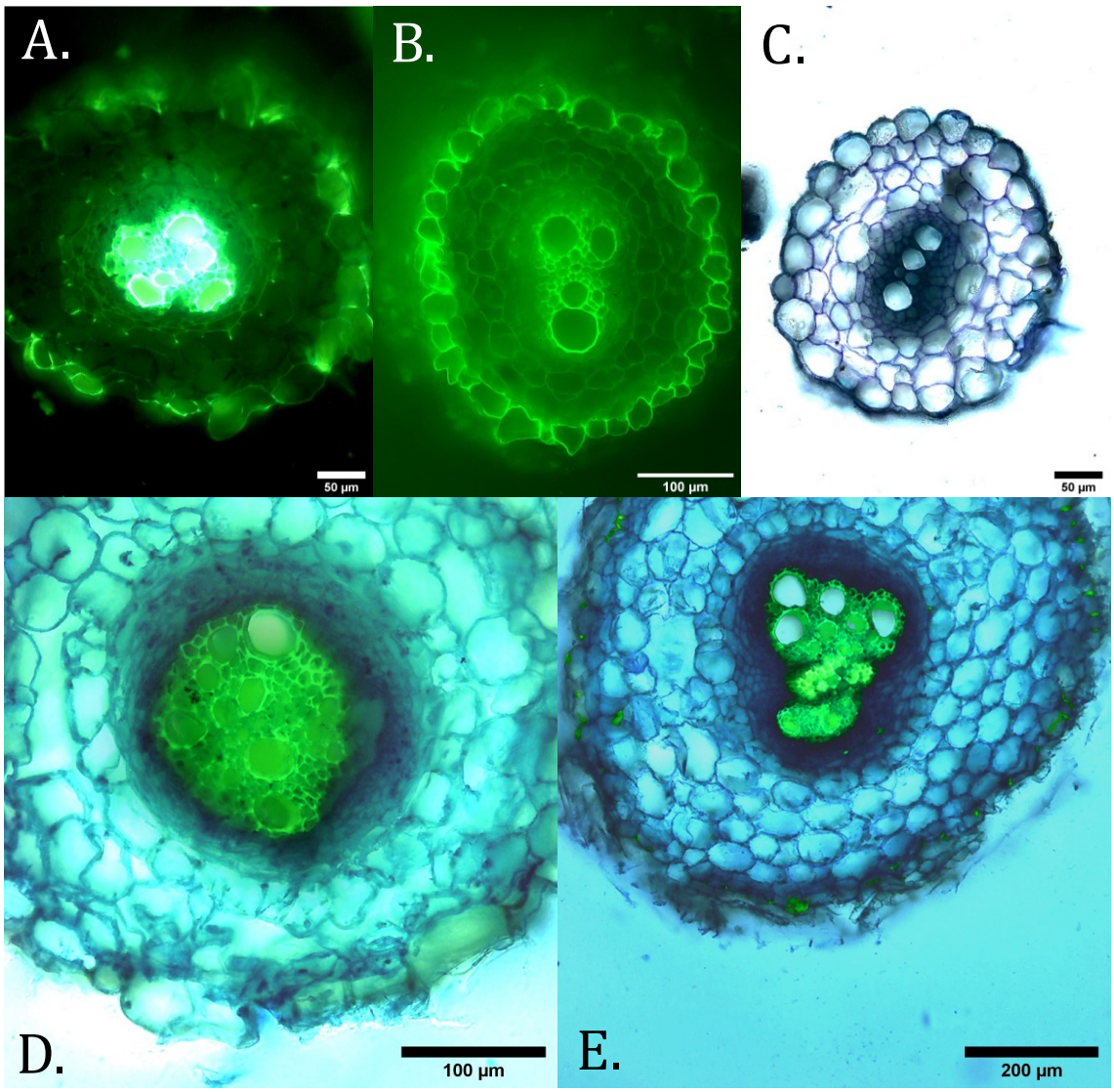

Figure 10 : Colorations used and examples of image composition. **A.** Coloration with Berberine-Aniline under UV. **B.** Coloration with Fluorol Yellow under UV. **C.** Coloration with Toluidine O under normal light. **D, E.** Mixed imaged composed of Berberine Aniline and Toluidine O staining.

For both naked samples of the first two segments and agar embedded samples, cross sections were made by hand with a razor blade. The sections were then stained with berberine-hemisulfate and aniline or with fluorol yellow. For each segment of roots, the cross sections were stored in Petri dishes in a drop of water

for berberine toluidine staining, and in a drop of 50% glycerol for fluorol yellow staining. Fast staining using only Toluidine O alone were also made for preliminary observations and additional cross sections (Yeung et al., 2015).

IV. A. 2. Berberine aniline staining

Berberine hemisulfate (BH), coupled with aniline, highlights lignin depositions, and therefore spots the Casparian strips (**Figure 10.A**). Following the Brundrett et al. (1988) and the Lux et al. (2005) protocol, BH 0,1% in water and aniline blue 0,5% in water solutions were prepared. Cross sections were first stained for 1h in BH, then rinsed in water and then stained in aniline blue for 30 minutes. The cross sections were rinsed again and post-stained with 0,05% toluidine O. The cross sections were mounted on lamellae and observed both using ultraviolet (UV) excitation (FITC or 488 excitation) and normal light using a Eclipse E400 (Nikon). Pictures were taken with a Moticam 2000 (Motic) and managed with Motic Image Plus (Motic).

IV. A. 3. Fluorol yellow staining

Fluorol Yellow (FY) highlights suberised tissues, like exodermis and metaxylem files (**Figure 10.B**). Kitin et al. (2020) recommends using it with glycerol as solvent. In addition to successfully dissolve FY, glycerol strengthens the samples, which makes cuts by hand easier, and the sample more resistant to degradation. The protocol of Lux et al. (2005) was followed for the preparation. A solution of 0,01% FY 088 in polyethylene glycol was heated at 90°C. Then a same volume of glycerol was added to the solution. One or two drops of the FY solution was placed on the cross-section samples, and the samples were stored a whole night. Then the samples were rinsed with water and observed with a microscope in a drop of 50% glycerol using UV excitation (FITC or 488 excitation).

Anatomical quantifications

IV. A. 4. Data measurement

Multiple pictures of a same cross section at different UV excitation were taken, and composed together with GIMP (GIMP development team, 2021) to get as much anatomical information as possible in one image. Indeed, cortex features were better identified with Toluidine 0 staining, where details about the stele were better highlighted with FY or BHS staining. The composed images were then quantified using the ImageJ software (Schneider et al., 2012).

Some assumptions and simplifications were made in the process of quantification. The objective was not to get a precise histological map, but rather to quantified tissues that could play a role in radial and axial water uptake. Tracheids and meta-xylem cells were quantified equally, and proto-xylem cells that are not yet differentiated were quantified as parenchyma cells. Primary phloem was difficult to spot, and therefore was not quantified but was rather supposed similar to parenchyma in terms of cell size and diameter. On the other hand, a secondary phloem layer appears quickly and was quantified. Vascular cambium was not considered as a specific tissue, as its features were similar to surrounding parenchyma and phloem and was therefore quantified as phloem or parenchyma.

The full quantification protocol consists of drawing a few cells for each tissue and measuring their size (in μm^2) or their width (in μm). For xylem, each vessel cell was drawn, because the number of xylem cells is a parameter of GRANAR, and it is obtained by counting the number of measurements. Regarding the parenchyma, phloem and cortex, cells were drawn along one or more radius, to avoid unintentional selection bias. For tissues that are composed of one single cell layer (pericycle, endodermis, exodermis and epidermis), a few cells were drawn in a random distribution along the arc of circle of the cell layer. For drawn cells of phloem, pericycle, endodermis, cortex, exodermis and epidermis, the cell width in the cross-section radius direction was measured. GRANAR generates round cells, whereas cells in these tissues appear to be elongated. We therefore chose to generate round cells in GRANAR but with a diameter equal to the width of the measured cells. By doing so, we end up with generated tissues that have more cells (that are round) in total, but with a diameter equal to the width of the measured cells in the direction of the cross-section radius. This choice was motivated by the fact that layer width has tremendous influence on radial water flow while the number of cells per cell layer (and by extension the number of cell walls for apoplastic pathway) have little effect.

The number of cell files within a tissue was stored as dedicated measures, and the hydrophobic stage of the endodermis and exodermis was recorded using notation *0* for no apoplastic barrier, *1* for Casparian bands and *2* for suberin lamellae.

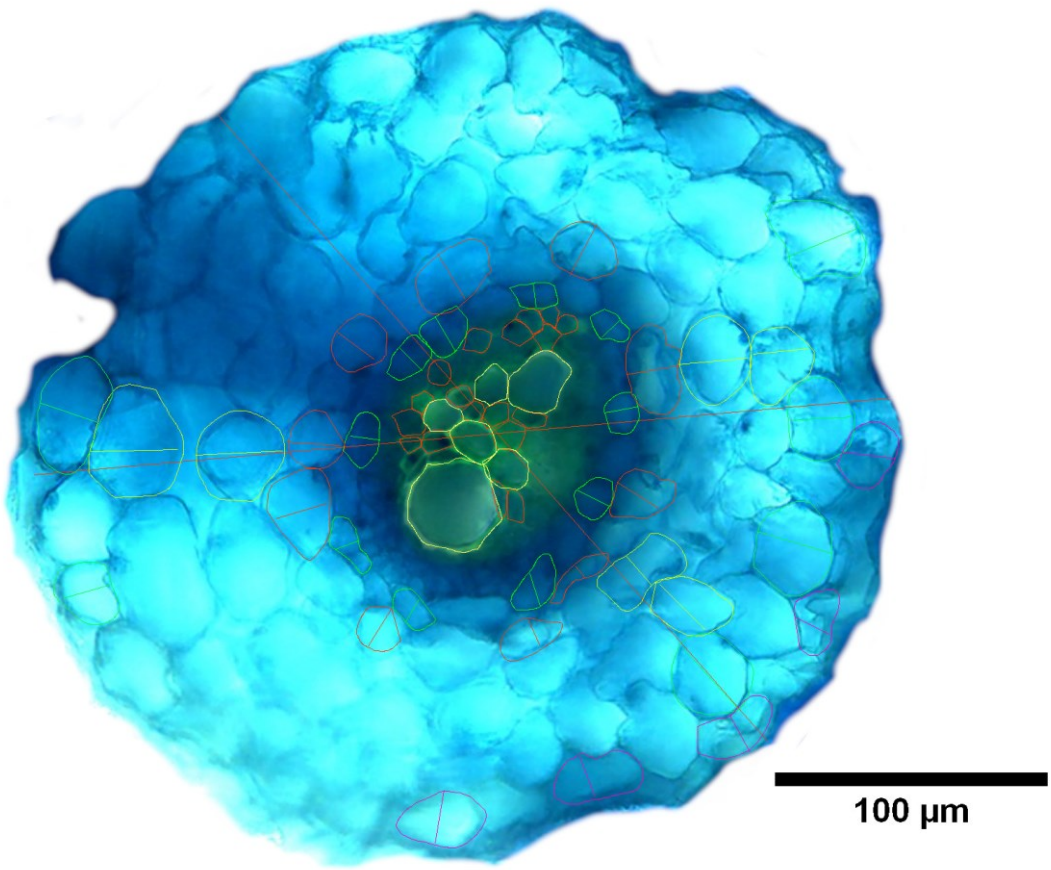

Figure 11 : Quantified cross-section picture. For each drawn cell, area was measured, and for each drawn segment (cell width, stele radius or cortex radius), the length was measured.

IV. A. 5. Data processing

All measurements of all pictures were stored in a database and treated in R (R Core Team, 2020) to get a table of the quantifications as GRANAR input parameters per plant and per segment. For the parameters that required treatment, a detailed explanation is given in this paragraph.

- For the inner stele (parenchyma), cells were considered as round, and the cell diameter parameter was computed using cell areas:

$$D_{cell,stele} = \frac{1}{n} \sum \left(2 \times \sqrt{\frac{area_i}{\pi}} \times 10^{-3} \right) \quad (4)$$

Where $D_{cell,stele}[mm]$ is the stele (parenchyma) cell mean diameter and $area_i$ [μm^2] is the area of the i^{th} measured cell and n is the number of measured cells.

- For the other tissues (pericycle, endodermis, cortex, exodermis and epidermis), the cell diameter was simple expressed as the mean of the cell diameter of the measured cells:

$$D_{cell} = \frac{1}{n} \sum 10^{-3} \times d_i \quad (5)$$

Where D_{cell} [mm] is the mean cell diameter, and d_i [μm] is the diameter of one cell among the n measured cells.

- For every tissue, the mean cell size was calculated as the mean of all cell areas within one tissue.

- Phloem proportion was computed as the ratio between phloem layer width and stele radius.

Data management

Architectural measures were stored in *csv* tables. Anatomical quantifications were recorded in a *xlsx* file for each cross section. One cross section is identified by the *id* of the plant, the segment, the zoom, and a repetition number. All quantifications were stored into a single *csv* file as the anatomical database (*Anatomy_full* table in the database). Then the data was processed into GRANAR input parameters and stored in the *Anatomy* table. **Figure 12** shows the complete database design used. This design allowed to perform statistical analysis, data process and model calibration while still feeding the database with new quantifications.

All codes used in this work can be found here: https://github.com/granar/granar_tomato

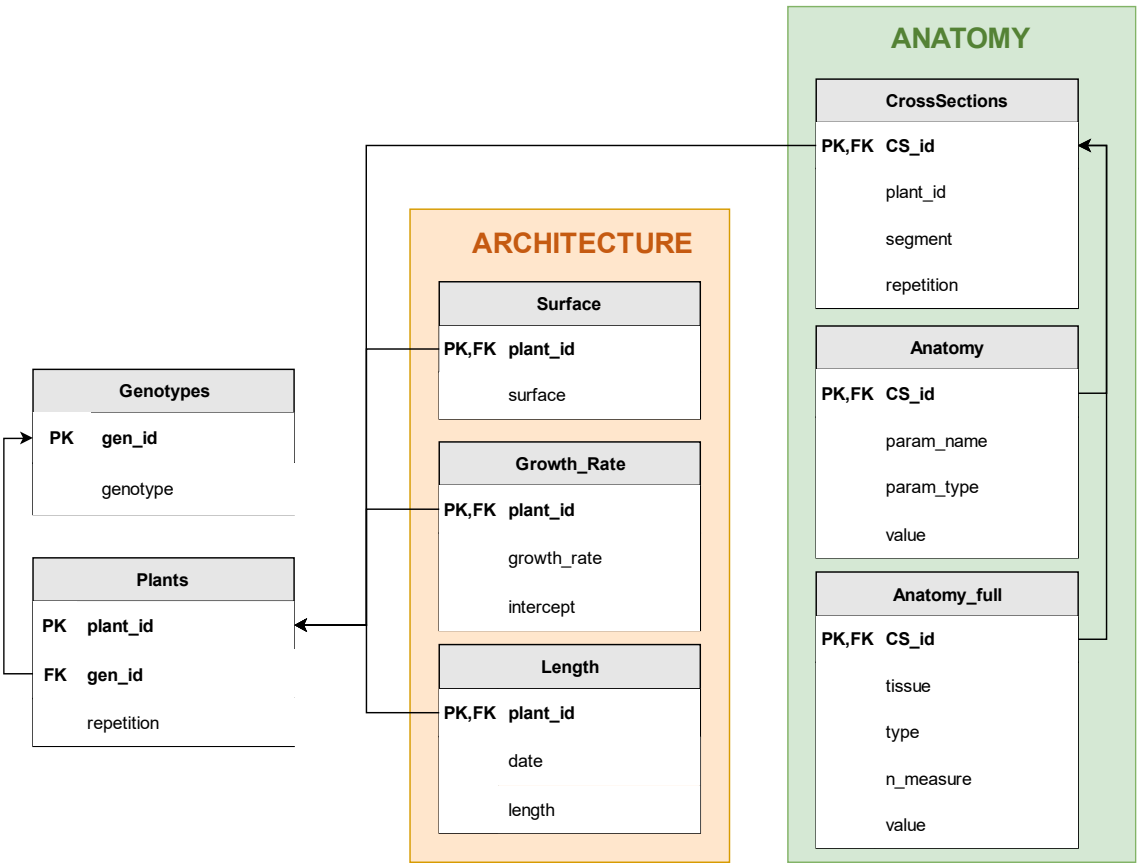

Figure 12 : Physical design of the database used.

Simulations

Remy Schoppach added new features and new functions to GRANAR by trying to fit the cross-section pictures taken and quantified in this master's thesis. The main feature that required changes was the generation of secondary xylem and phloem.

The initial version of GRANAR generated metaxylem blades of one cell width, but the observed pattern of xylem was more like a random distribution within the stele. A new function was coded to fill the stele with parenchyma cells and to place xylem files in a more realistic pattern of early secondary growth. In addition, modifications of the code were made to create multiple cell files of phloem.

First, the inner stele is filled with parenchyma. The number of parenchyma cells is determined based on the inner stele area $A_{inner\ stele}$ [μm^2], the total xylem area A_{xylem} [μm^2] and the mean parenchyma cell size $\overline{CS}_{parenchyma}$ [μm^2]:

$$n_{parenchyma} = \frac{A_{inner\ stele} - A_{xylem}}{\overline{CS}_{parenchyma}} \quad (6)$$

Where the total xylem area A_{xylem} is the product of the mean xylem cell size and the number of xylem vessels, while the inner stele area is extracted from the diameter:

$$A_{inner\ stele} = \pi \left(1000 \times \frac{D_{stele} - 2\,\overline{CD}_{pericycle}}{2} \right)^2 \quad (7)$$

Where $D_{stele}[\mu m]$ is the stele diameter and $\overline{CD}_{pericycle}$ [μm] is the mean cell diameter of the pericycle.

For the xylem cells, the number of generated cells is an input parameter. The sizes of the cells are randomly picked following a beta distribution of parameters $\alpha = 2$ and $\beta = 4$ in a range between 0 and the maximum xylem cell size (set in input) using the *rBeta2009* package[4]. The positioning of the centre of xylem vessels in the stele is done with the function *circleProgressiveLayout* of the *packcircle* package[5]. Then the centre of xylem cells and parenchyma cells are randomly mixed in the inner stele.

In the initial version of GRANAR, the phloem was generated as poles between xylem blades. However, in young secondary growth, phloem appeared to be organised as a full layer of cells around the parenchyma and inner of the pericycle. Here we first fill the inner stele only with parenchyma and then we assign the outermost layers as phloem. The phloem area $A_{phloem}[\mu m^2]$ is computed based on the fraction of phloem f_{phloem} in the stele along one stele radius $r_{inner\ stele}$ [mm] :

$$A_{phloem} = \pi \left(\frac{r_{inner\ stele}\, f_{phloem}}{1000} \right)^2 = f_{phloem}^2 \times A_{inner\ stele} \quad (8)$$

Finally, the other tissues are generated with the initial GRANAR code and the Voronoi tessellation creates the cell walls.

[4] https://rdocumentation.org/packages/rBeta2009
[5] https://rdocumentation.org/packages/packcircles

V. Results

Architectural and anatomical characterization

Since Moneymaker is a widely used domestic cultivar that has been optimised for crop production while *S. pimpinellifolium* is a wild species that grow in natural environments, differences in grow and water uptake strategies are expected. These strategies are reflected by architectural and anatomical traits.

V. A. 1. Architecture

In this experiment, there were no significant differences among *S. pimpinellifolium* accessions in terms of growth rate and leaf surface (**Table 2**). All *S. pimpinellifolium* plants were then grouped as "wild" tomato and compared to *S. lycopersicum* Moneymaker as "domestic" tomato. *S. pimpinellifolium* leaf surface was significantly lesser than Moneymaker. The evolution of the maximum root length through time was visually modelled using a quadratic regression (**Figure 13.C**) using four measurement points. Yet, the quadratic regression was not much better than a linear regression (respectively $R^2 = 0.6774$ and $R^2 = 0.6699$) so the slope of the linear regression was used as the growth rate parameter. For each plant, the mean growth rate was computed, and Moneymaker showed significantly lower growth rate than *S. pimpinellifolium.* By comparing growth rate and leaf area, **Figure 13.D** clearly shows that *S. pimpinellifolium* and Moneymaker presents different strategies: while Moneymaker allows more carbon in leaves, *S. pimpinellifolium* focus on root development. This suggests that S. pimpinellifolium could have lesser evapotranspiration, but that it might have a better access to soil water.

V. A. 2. Anatomical characterization

Each root segment was characterised and quantified. **Table 3** shows a summary of the features of each segment. All the quantified cross sections showed metaxylem cells coupled with parenchyma in a "random" filling of the centre of the stele, losing the arch nature of xylem blades. An exception can be made for very young roots segments, where two xylem blades can be seen near the tip, but we did not focus on that stage.

Apoplastic barriers (suberin lamellae and Casparian strips) were spotted with specific colorations. By paying attention to the appearance of barriers in each segment, we can build a map of apoplastic structures along the main root, as shown in **Figure 14**. For very young roots in primary growth, Casparian bands can sometimes be seen in exodermis, while endodermis presents no apoplastic structures.

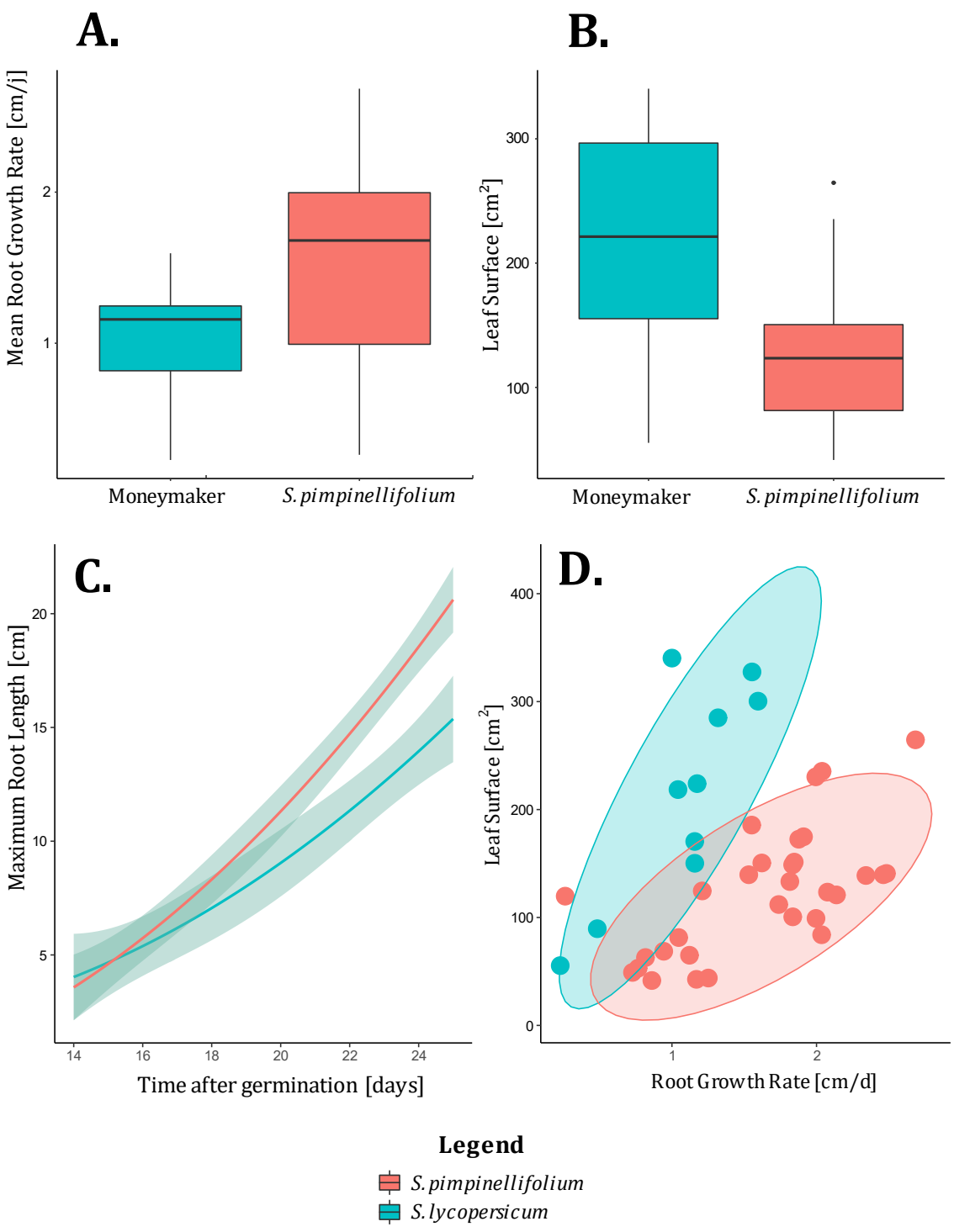

Figure 13 : Architectural results for *S. pimpinellifolium* (orange) and *S. lycopersicum* (green). **A.** Mean root growth rate. **B.** Leaf surface. **C.** Leaf surface vs. root growth rate.

Table 2 : Results of analysis of the variance for leaf surface and growth rate.

Parameter	Accessions/Species	Comparison
Leaf surface	*S. pimpinellifolium* accessions	F = 0.8 Pr (>F) = 0.53
	S. pimpinellifolium VS *S. lycopersicum*	F = 13.7 Pr (>F) < 0.001
Growth Rate	*S. pimpinellifolium* accessions	F = 0.59 Pr (>F) = 0.67
	S. pimpinellifolium VS *S. lycopersicum*	F = 6.87 Pr (>F) = 0.012

In segment 4, we see a suberised exodermis while endodermis begins to form Casparian bands (**Figure 14**.A. and B.). Segment 3 shows both exodermis and endodermis with suberin (**Figure 14**.C). In the pictures of segment 2 (**Figure 14**.D) suberin was highlighted in exodermis but was not visible in endodermis. We make the hypothesis that in that segment the endodermis is also suberised but with no visual proof. Indeed, it seems unlikely that this region is not suberised while the previous segments are.

Table 3 : Summary of the features of each segment

Segment	**Features**	**Localisation**
Segment 1	Interface between root and shoot, Secondary growth, Central pith, Stele radius > cortical radius	Near the collar. 10-15 cm from the tip.
Segment 2	Secondary growth, Stele radius > cortical radius	8-10 cm from the tip
Segment 3	Young secondary growth, Stele radius ~ cortical radius	6-8 cm from the tip
Segment 4	End of primary growth, Stele radius < cortical radius, Few meta-xylem cells in random disposition around the centre of the stele	2-6 cm from the tip
Segment 5 (qualitative)	Primary growth, Xylem in 2 blades	0-2 cm from the tip

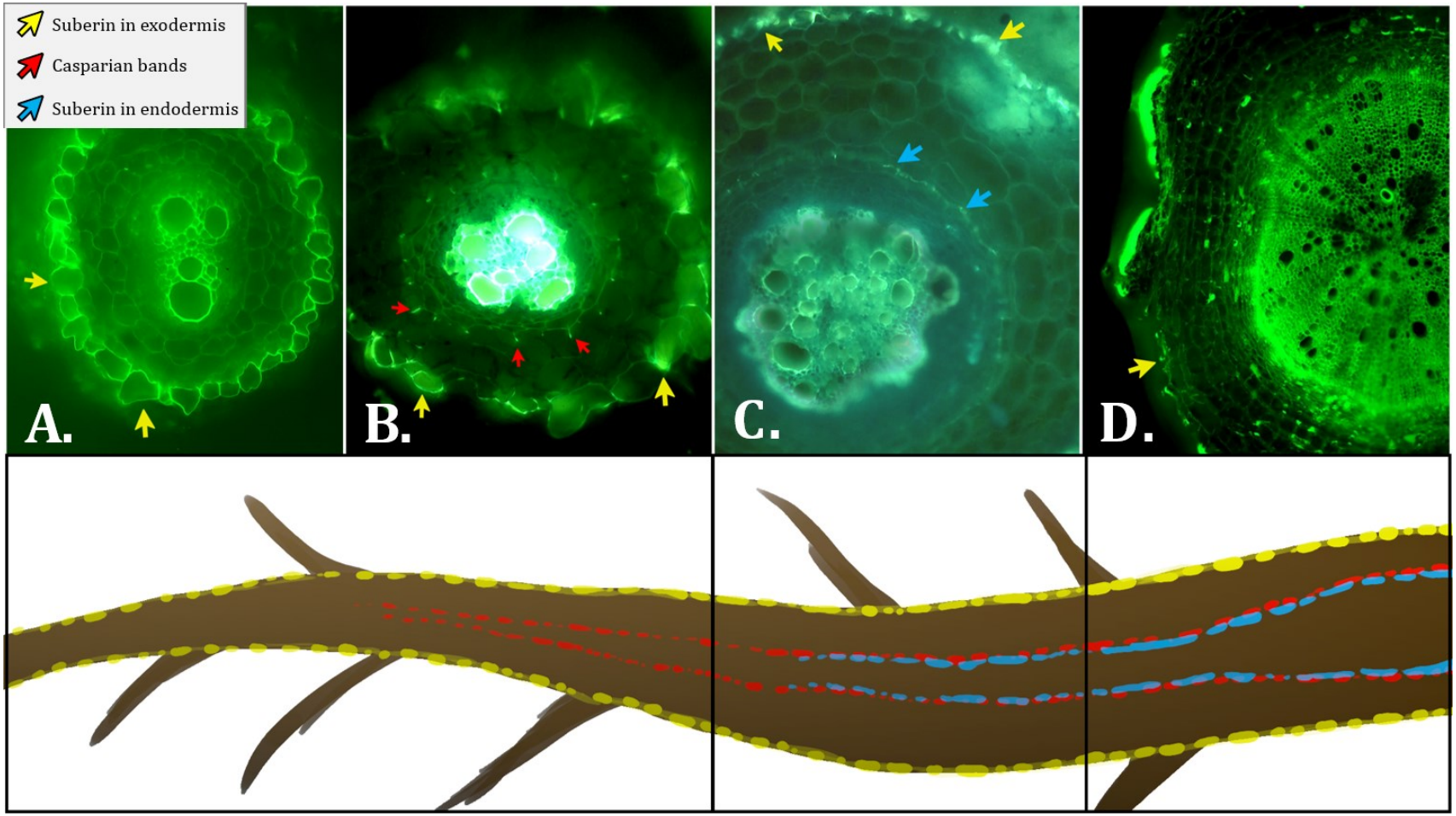

Figure 14 : Apoplastic barriers along the root. Yellow is for suberin in exodermis, red is for Casparian bands in endodermis and blue is for suberin in endodermis. **A.** Segment 4 whith suberised exodermis and no barrier in endodermis. **B.** Segment 4 with suberised exodermis and Casparian strips in endodermis. **C.** Segment 3 with suberised exodermis and endodermis. **D.** Segment 2 with suberised exodermis and hypothetical suberised endodermis.

A surprising feature is the missing of a clear epidermis in the pictures. Even in early stages, epidermis cells were small and rare, and the exodermis seems to rapidly become the outermost tissue. However, some pictures clearly show a distinct epidermis layer, and proved that suberin comes from the exodermis and are not diffuse in epidermis (**Figure 15**). A hypothesis could be that in hydroponics, plants do not need epidermis to explore solid matter, and therefore sacrifice epidermis to increase water and nutrient uptake from the solution.

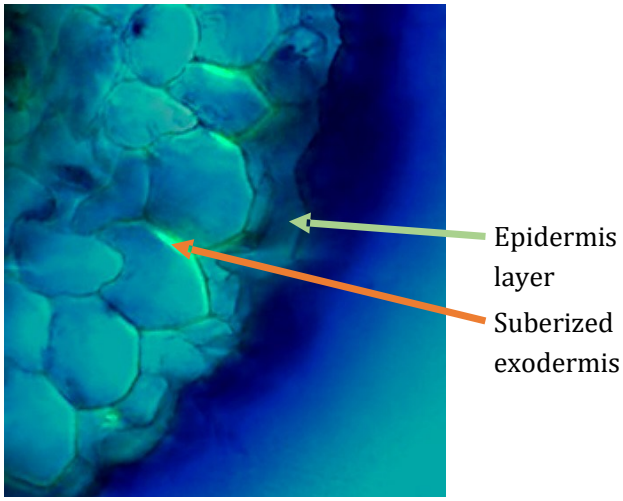

Figure 15 : Exodermis and epidermis in segment 4.

Due to a lack of time and substantial number of lost samples in the process of elaborating the protocol, only two genotypes were fully studied and quantified in terms of anatomy — *S. pimpinellifolium* LA0114 and *S. lycopersicum* Moneymaker. From characterising anatomy among multiple genotypes, the project turned into the making of a quantification protocol and a focus was placed on the update of GRANAR. This choice was also motivated by the absence of significant difference in architecture in *S. pimpinellifolium* accessions. For both cultivars analysed, 4 roots were used, and each root was divided in 4 segments, for a total of 24 quantified cross sections. Each quantification takes between 20 and 40 min (with image process and composition). At least one cross section of each segment of each root was quantified, except for the first segment corresponding to the interface between root and shoot, where the anatomy changes too hardly to be quantified with the same protocol.

V. A. 3. Quantification of the anatomy

Anatomical quantification shows that all traits are correlated, except the proportion of phloem in the stele (**Figure 16.D**). All traits present significant differences between the different segments (except epidermis), with increasing values from the bottom (Segment 4) to the top of the root (Segment 2). In terms of differences between *S. pimpinellifolium* and Moneymaker, only xylem and cortex traits (specially xylem mean size, xylem total area, cortex cell diameter and cortex layer diameter) are significatively different at a level of 0.05. Xylem total area was computed by multiplying the number of vessels by the mean vessel size. The cortex layer diameter is obtained by multiplying the mean cell diameter by the number of layers.

Table 4 : Analysis of variance for the effect of the segment and the effect of the genotype

Tissue	Trait	Effect of the segment		Effect of the genotype	
		F value	P value	F value	P value
Xylem	number of files	32.9	< 10e-3	2.9	0.1046
Xylem	mean cell size	11.4	< 10e-3	4.4	0.05
Xylem	total area (log)	45	< 10e-3	5.9	0.025
Stele	total area (log)	44.2	< 10e-3	0.5	0.408
Stele	layer diameter	23.9	< 10e-3	0.13	0.71
Parenchyma	mean cell size	22.7	< 10e-3	0.21	0.648
Cortex	mean cell diameter	37.9	< 10e-3	5.4	0.031
Cortex	number of layers	3.59	0.0487	0.81	0.17
Cortex	layer diameter	20.54	< 10e-3	6.38	0.022
Phloem	number of files	10.28	0.00105	0.0613	0.81
Phloem	max cell size	46.34	< 10e-3	1.294	0.27
Phloem	proportion	3.77	0.043	0.006	0.93
Pericycle	cell diameter	32.29	< 10e-3	0.09337	0.7
Endodermis	cell diameter	22.54	< 10e-3	1.43	0.24
Exodermis	cell diameter	6.96	0.005	0.39	0.53
Epidermis	cell diameter	0.95	0.3921	0.03	0.866

Interestingly, we can compare the mean layer diameter of the stele and the cortex. In early segments, stele and cortex have equal layer diameter, but in the older segments, the stele diameter overtakes the cortex diameter till being twice bigger (**Figure 16.C**). This is due to the secondary growth pattern in which the stele growth by generation of secondary xylem and phloem and put pressure on the cortex layers.

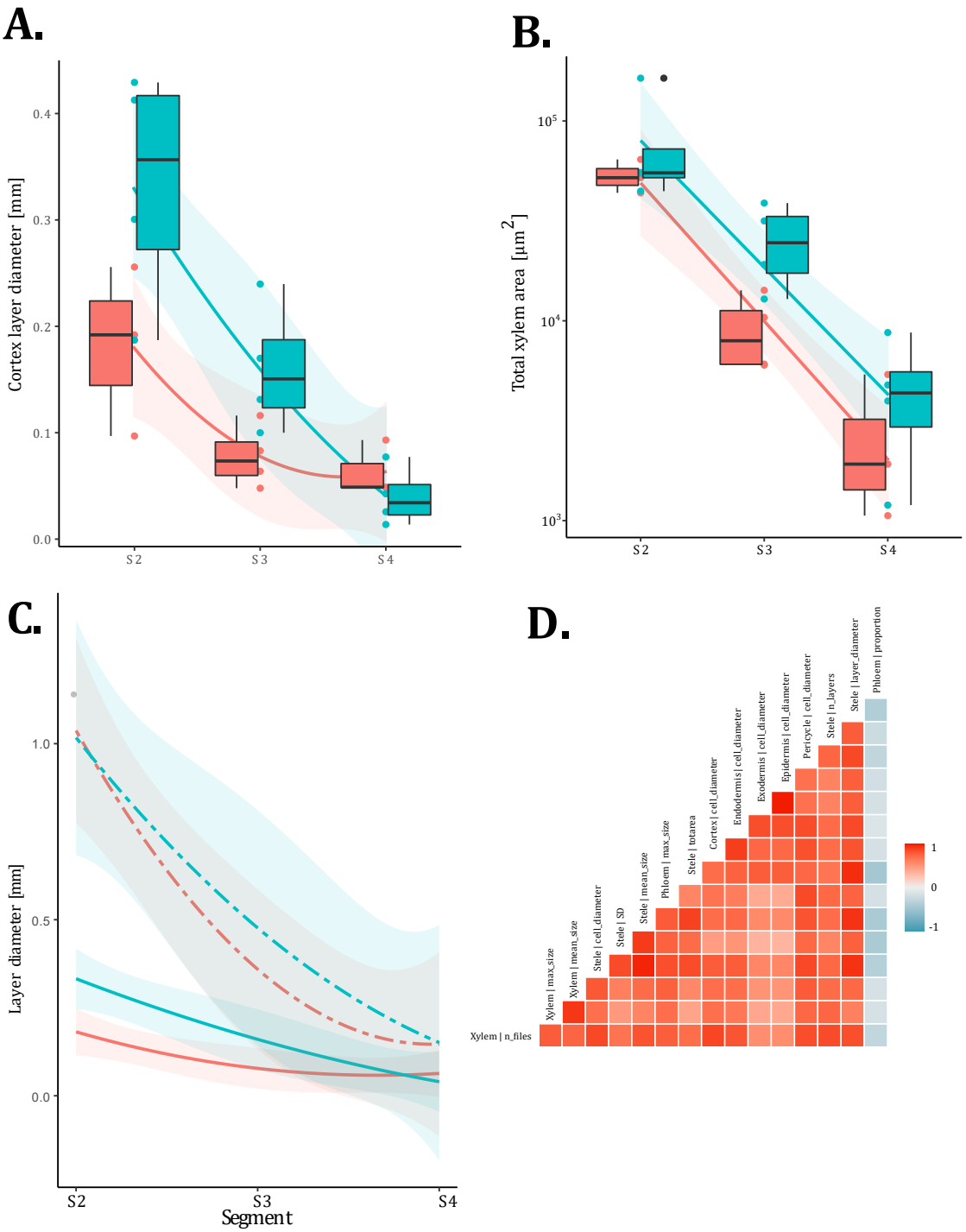

Figure 16 : Visualisation of anatomical quantifications. Orange is for *S. pimpinellifolium,* and green is for *S. lycopersicum.* **A.** Cortex layer diameter. **B.** Total xylem area. **C.** Comparison of the stele layer diameter (dotted lines) and cortex layer diameter (straight lines) along the root. **D.** Heatmap of the correlations between traits.

GRANAR secondary growth update: Pack Xylem function

The updated version of GRANAR simulates cross sections that contain secondary growth patterns. The parameters of the update of GRANAR are presented in **Table 5**. The secondary growth module is a set of R functions called Pack Xylem that can be directly integrated to the main code of GRANAR. The user can now choose to generate dicotyledonous root cross sections in primary stage or in secondary growth stage (**Figure 17**). Some little issues still have to be fixed, like a mismatch between parenchyma, phloem and endodermis for some cells (cfr Appendix 2 : Example of secondary growth cross sections generated with the update of GRANAR).

The maturity stages of the endodermis and the exodermis are represented in input by three stages: 0) no apoplastic barrier, 1) Casparian strip, 2) suberin lamellae. These inputs do not change the anatomical generation but are important for the future computing of water flow with MECHA.

Water uptake

A modified version of MECHA was coded by Valentin Couvreur[6], corresponding to the different hydrophobic stages of endodermis and exodermis. Unfortunately , we could not yet link GRANAR with MECHA and compute water flow in this master's thesis due date.

[6] ELIA, UCLouvain

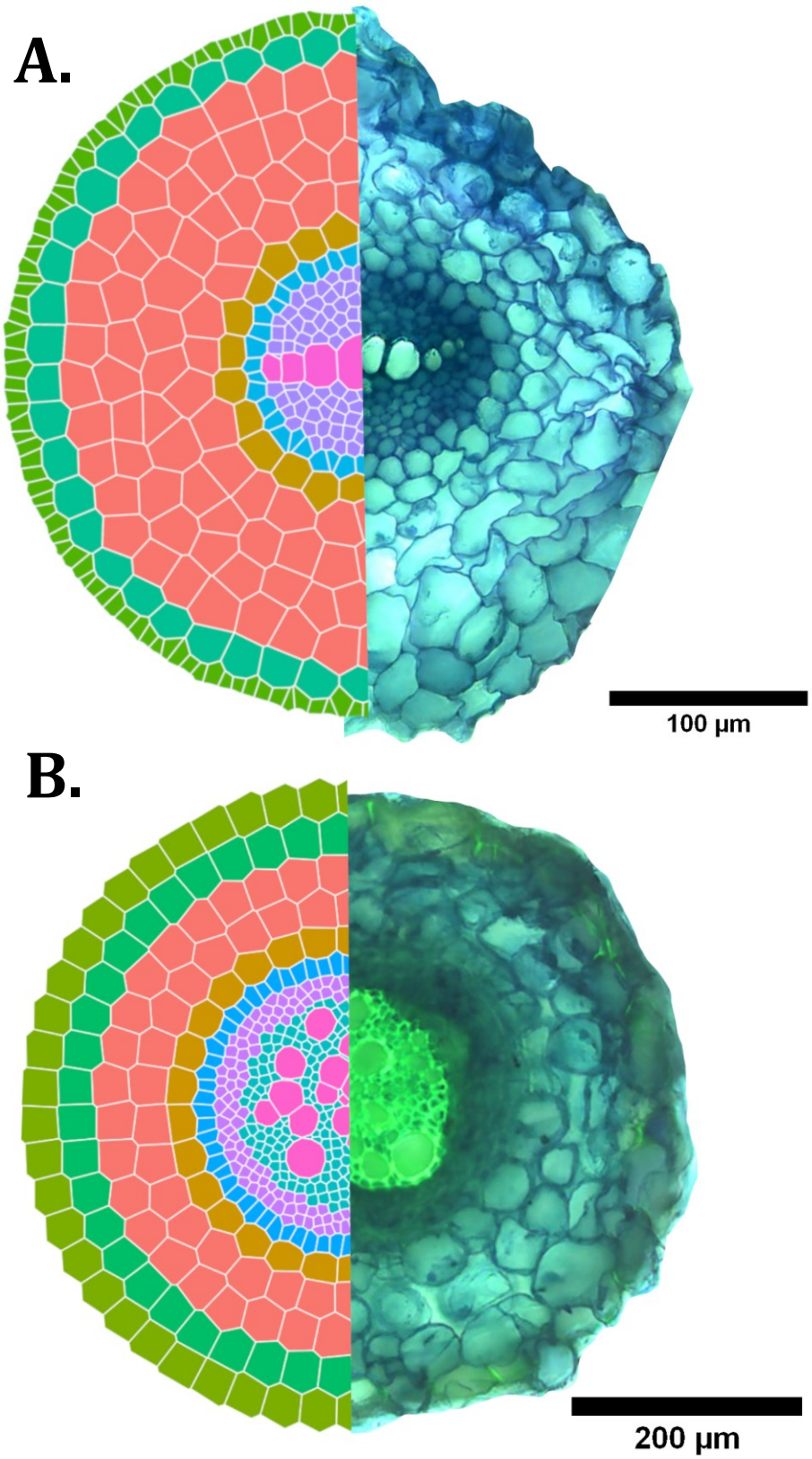

Figure 17 : Comparison side by side between generated cross section and corresponding anatomy picture. **A.** Initial version of GRANAR vs. primary growth cross section. **B.** Update of GRANAR vs. young secondary growth cross section.

Table 5 : Parameters of the update of GRANAR.

Name/Tissue	Type	Description	Range/units
Secondary growth	Parameter	Activate or deactivate generation of secondary growth patterns	0 or 1
Randomness	Parameter	Set the level of randomness in the generation	0 to 5
Plant type	Parameter	Choose to generate dicotyledon or monocotyledon	1 for monocots, 2 for dicots
Aerenchyma	Proportion	Set the proportion of aerenchyma	[−]
Aerenchyma	N_files	Set the number of aerenchyma files	[−]
Xylem	Max_size	Set the maximum size of xylem cells	$[\mu m^2]$
Xylem	Mean_size	Set the mean size of xylem cells	$[\mu m^2]$
Parenchyma	Cell_diameter	Set the mean diameter of parenchyma cells	$[mm]$
Stele	SD	Set the standard deviation of parenchyma cell size	$[\mu m^2]$
Stele	Totarea	Set the total area of the stele (containing parenchyma, xylem, phloem and pericycle)	$[\mu m^2]$
Parenchyma	N_layers	Set the number of cell layers	[−]
Stele	Layer_diameter	Set the diameter of the stele	$[mm]$
Phloem	Max_size	Set the maximum size of phloem cells	$[\mu m^2]$
Phloem	N_files	Set the number of phloem files	[−]
Phloem	Proportion	Set the proportion of phloem in the stele	[−]
Pericycle	Cell_diameter	Set the mean pericycle cell diameter	[mm]
Pericycle	N_layers	Set the number of pericycle files	[−]
Endodermis	Cell_diameter	Set the mean endodermis cell diameter	[mm]
Endodermis	N_layers	Set the number of endodermis files	[−]
Endodermis	Barrier	Set the maturity stage of cells	0 : no apoplastic barrier; 1 : Casparian strips; 2 : Suberin lamellae
Cortex	Cell_diameter	Set the mean cortex cell diameter	$[mm]$
Cortex	N_layers	Set the number of cortex files	[−]
Exodermis	Cell_diameter	Set the mean exodermis cell diameter	[mm]
Exodermis	N_layers	Set the number of exodermis files	[−]
Exodermis	Barrier	Set the maturity stage of cells	0 : no apoplastic barrier; 1 : Casparian strips; 2 : Suberin lamellae
Epidermis	Cell_diameter	Set the mean epidermis cell diameter	[mm]
Epidermis	N_layers	Set the number of epidermis files	[−]

VI. Discussion & perspectives

Anatomy and comparison between species/genotypes

It is clear that the number of samples used in this work is not enough to formulate strong conclusions and differentiate physiological behaviour between wild and domestic tomato species. Instead, the manipulations served to update microscopical protocols, quantification process and simulation tools. The comparison between genotypes must therefore stay anecdotal.

Yet some interesting features were consistently observed in the cross sections. First, the fact that exodermis suberisation appears before the endodermis one probably has consequences on water uptake. Second, the shift in layer diameter of stele and cortex is intriguing from a water dynamic point of view. A larger stele would increase the radial conductivity by extending the water pathway area and an increased xylem area, but is it inhibited by the development of apoplastic barriers? Larger xylem area is supposed to increase axial conductivity, so how the shift in radial to axial conductivity will happen? Hopefully, these questions can be investigated with the new version of GRANAR and a link with MECHA.

A protocol to quantify dicot anatomy and influent traits

Multiple techniques were tested, coming both from the working environment and from literature, to formulate a protocol for quantifying anatomical traits, apoplastic barriers, tissue development, secondary growth patterns and maturation stages. In particular, colorations of updated protocols from Brundrett et al. (1988), Kitin et al. (2020) and Lux et al. (2005) were coupled with moult embedding techniques from Atkinson and Wells (2017) and Zelko et al. (2012) to quantitatively investigate anatomy along the roots, from the tip to the collar. The final pictures were clean and information rich. Nevertheless, good sample colorations require lots of time (~2h for BH and ~20h for FY), so meticulous organization is required to deal with a high number of samples.

Studying the evolution of the anatomy along the root is not obvious, and some simplifications had to be made. While Heymans et al. (2021) achieved a nice precision and a characterisation of the anatomy along multiple root types, here anatomy was evaluated in 3 segments of the main root, that presented specific patterns, similar to the methodology of Gambetta et al. (2013).

Secondary growth update of GRANAR

The implementation of new GRANAR modules to simulate dicots is a step towards high throughput modelling of water flow in roots. However, the link with MECHA is not yet functional, and requires to code new sections, investigate

subcellular parameters for tomato, and validate radial and axial water flow computations with literature data.

GRANAR is able to generate cross sections for studying water flow, but does not consider some tissues, like cambium or periderm that were not supposed to play a significant role in water dynamics or that simply not appear at all in tomato. Thus, updates are required to enhance the fidelity of the model to reality. One possible future for GRANAR is the construction of a developmental module, as mentioned by Heymans et al. (2020). Especially for dicots, the initial version of GRANAR can simulate young primary growth anatomies, while the new version can generate large sections in secondary growth. So far, the generation of anatomy along a root was done by generating "step" cross-sections and by interpolation, but coupling the two dicot versions of GRANAR with a progressive development (cell division with hormonal growth control and response) along the root might help explore the consequences of anatomical development on nutrient uptake. Needless to say, that will add tremendous complexity to the model and hard time for future developers and users.

Perspectives

The quantification protocol established in this master's thesis works well, using microscope techniques, different colorations, computational tools to measure traits, a database design, and codes to load, treat and display data at low cost. All these tools and techniques can now be applied to a larger set of samples, e.g. to other tomato species, more genotypes, and more repetitions. Obviously, experimental design will have to be more complicated than the one used in this work. Indeed, environmental factors, interactions and other parameters influencing the variance that was not considered in this work will have to be included. Nevertheless, experimental protocols to study root anatomy "by hand" still remain highly time consuming. There is therefore a large place for innovation, and integration of new technologies to reduce the manipulation duration and improve quality of samples. About trait quantification from cross-section pictures, new computational tools using image analysis and machine learning concepts could be specifically developed to dicots in order to increase the productivity, like RootScan do for maize. On the other hand, coupling the new version of GRANAR with MECHA will open the way to multiscale modelling of water flow in tomato, or similar dicots (e.g. grapevines).

These anatomical phenotyping tools (both experimental and computational) could be coupled to architectural phenotyping process, to enhance the complexity of the simulations and affine our understanding of plant water uptake. Several applications exist, like test the effects of combinations of microscopic and macroscopic traits on water flow, simulate the anatomical response to stress and investigate the water dynamic consequences, or simulate the anatomical behaviour of roots in different soils and environments.

Personal enrichment and perspectives

Root anatomy is a deep and fascinating world. Its inaccessibility makes it full of mysteries and wonders. I spend a tremendous time of this master's thesis to learn the cross-section art, and I am proud of the nice pictures I eventually made. I paid lots of attention to the data management and the design of codes, to build a solid and adjustable pipeline of data collection, process, and export. Unfortunately, I could not apply these techniques to a set of samples large enough to get significant data and conclusions. The comparison between wild and domestic tomato still remains anecdotal. However, the skills that I developed and the tools that we made can now be apply to a large set of plants and constitute the basis for a new project.

VII. Conclusion

Understand the role of plant traits on water uptake is crucial in a climate change context, where droughts that impact crop production are expected to be more frequent and more severe. Root architectural traits are subject to a large number of phenotyping projects. At the lower scale, root anatomy plays a major role in water dynamics, and coupling anatomical traits with architectural traits in phenotyping processes might improve our understanding of water-saving strategies in plants. However, anatomy is difficult to study with high throughput due to its microscopical scale. New tools and protocols have to be developed to enhance the quality of anatomical modelling, and to integrate anatomy into plant-scale simulations.

In this work, we extended the work of Heymans et al. (2020) by adding a secondary growth module to the generator of root anatomy GRANAR. For that, we used tomato as model plant. We grew tomato in hydroponics, monitored architectural parameters, and explored tomato root anatomy. Staining techniques were tested and apply, and a protocol for anatomy quantification was built. Tomato root anatomy was characterised, and maturity stages along the tap root were investigated.

Two species of tomato were studied and compared, but the results cannot be exploited as a conclusion, due to not enough repetitions and genotypes used. However, it was sufficient to characterise general root tomato anatomy and obtain useful quantifications.

With the collected data, we implemented and validated the new R function Pack Xylem, that is integrated in the code of GRANAR and allows the generation of anatomical secondary growth patterns. The virtual cross sections generated with this new module are compatible with MECHA, the radial root hydraulic solver.

The next step of this master's thesis will be to perform sensitivity analysis of the influence of secondary growth features on water flow, by linking GRANAR and MECHA. This will open the gates for new applications, e.g. include the new version of GRANAR into VIPER, the virtual phenotyping pipeline for root hydraulic traits, to study the influence of local anatomical and hydraulic parameters on global plant water dynamics.

References

Al-Khayri, J.M., Jain, S.M., Johnson, D.V. (Eds.), 2021. Advances in Plant Breeding Strategies: Vegetable Crops: Volume 9: Fruits and Young Shoots. Springer International Publishing, Cham. https://doi.org/10.1007/978-3-030-66961-4

Arafa, A., 2015. Secondary Growth Pattern In The Roots Of Two Herbaceous Species Belonging To Genus Solanum. Journal of Plant Production 6, 1679–1691. https://doi.org/10.21608/jpp.2015.52079

Atkinson, J.A., Pound, M.P., Bennett, M.J., Wells, D.M., 2019. Uncovering the hidden half of plants using new advances in root phenotyping. Current Opinion in Biotechnology 55, 1–8. https://doi.org/10.1016/j.copbio.2018.06.002

Atkinson, J.A., Wells, D.M., 2017. An Updated Protocol for High Throughput Plant Tissue Sectioning. Front. Plant Sci. 8, 1721. https://doi.org/10.3389/fpls.2017.01721

Bedinger, P.A., Chetelat, R.T., McClure, B., Moyle, L.C., Rose, J.K.C., Stack, S.M., van der Knaap, E., Baek, Y.S., Lopez-Casado, G., Covey, P.A., Kumar, A., Li, W., Nunez, R., Cruz-Garcia, F., Royer, S., 2011. Interspecific reproductive barriers in the tomato clade: opportunities to decipher mechanisms of reproductive isolation. Sex Plant Reprod 24, 171–187. https://doi.org/10.1007/s00497-010-0155-7

Bigot, S., Pongrac, P., Šala, M., van Elteren, J.T., Martínez, J.-P., Lutts, S., Quinet, M., 2022. The Halophyte Species Solanum chilense Dun. Maintains Its Reproduction despite Sodium Accumulation in Its Floral Organs. Plants 11, 672. https://doi.org/10.3390/plants11050672

Blanchard-Gros, R., Bigot, S., Martinez, J.-P., Lutts, S., Guerriero, G., Quinet, M., 2021. Comparison of Drought and Heat Resistance Strategies among Six Populations of Solanum chilense and Two Cultivars of Solanum lycopersicum. Plants 10, 1720. https://doi.org/10.3390/plants10081720

Brundrett, M.C., Enstone, D.E., Peterson, C.A., 1988. A berberine-aniline blue fluorescent staining procedure for suberin, lignin, and callose in plant tissue. Protoplasma 146, 133–142. https://doi.org/10.1007/BF01405922

Burton, A.L., Williams, M., Lynch, J.P., Brown, K.M., 2012. RootScan: Software for high-throughput analysis of root anatomical traits. Plant Soil 357, 189–203. https://doi.org/10.1007/s11104-012-1138-2

Chandrasekhar, A., Julkowska, M.M., 2022. A Mathematical Framework for Analyzing Wild Tomato Root Architecture. Journal of Computational Biology 29, 306–316. https://doi.org/10.1089/cmb.2021.0361

Chaumont, F., Tyerman, S.D., 2014. Aquaporins: Highly Regulated Channels Controlling Plant Water Relations. Plant Physiology 164, 1600–1618. https://doi.org/10.1104/pp.113.233791

Chimungu, J.G., Brown, K.M., Lynch, J.P., 2014. Large Root Cortical Cell Size Improves Drought Tolerance in Maize. Plant Physiol. 166, 2166–2178. https://doi.org/10.1104/pp.114.250449

Conesa, M.À., Muir, C.D., Roldán, E.J., Molins, A., Perdomo, J.A., Galmés, J., 2017. Growth capacity in wild tomatoes and relatives correlates with original climate in arid and semi-arid species. Environmental and Experimental Botany 141, 181–190. https://doi.org/10.1016/j.envexpbot.2017.04.009

Couvreur, V., Faget, M., Lobet, G., Javaux, M., Chaumont, F., Draye, X., 2018. Going with the Flow: Multiscale Insights into the Composite Nature of Water Transport in Roots. Plant Physiol. 178, 1689–1703. https://doi.org/10.1104/pp.18.01006

Das, A., Schneider, H., Burridge, J., Ascanio, A.K.M., Wojciechowski, T., Topp, C.N., Lynch, J.P., Weitz, J.S., Bucksch, A., 2015. Digital imaging of root traits (DIRT): a high-throughput computing and collaboration platform for field-based root phenomics. Plant Methods 11, 51. https://doi.org/10.1186/s13007-015-0093-3

Doussan, C., 1998. Modelling of the Hydraulic Architecture of Root Systems: An Integrated Approach to Water Absorption—Distribution of Axial and Radial Conductances in Maize. Annals of Botany 81, 225–232. https://doi.org/10.1006/anbo.1997.0541

Draye, X., Thaon, P., Ligeza, A., Lobet, B., Lobet, G., Civava, R., De Vleeschouwer, C., 2018. High Throughput Root Phenotyping in Aeroponics : one step from seed to root growth parameters. Presented at the International Society of Root Research, ELIA, UCLouvain, Israel.

Duncan, K.E., Czymmek, K.J., Jiang, N., Thies, A.C., Topp, C.N., 2022. X-ray microscopy enables multiscale high-resolution 3D imaging of plant cells, tissues, and organs. Plant Physiology 188, 831–845. https://doi.org/10.1093/plphys/kiab405

Enstone, D.E., Peterson, C.A., Ma, F., 2002. Root Endodermis and Exodermis: Structure, Function, and Responses to the Environment. J Plant Growth Regul 21, 335–351. https://doi.org/10.1007/s00344-003-0002-2

FAO, 2022. Land & Water, Tomato [WWW Document]. URL https://www.fao.org/land-water/databases-and-software/crop-information/tomato/fr/ (accessed 7.9.22).

Gambetta, G.A., Fei, J., Rost, T.L., Knipfer, T., Matthews, M.A., Shackel, K.A., Walker, M.A., McElrone, A.J., 2013. Water Uptake along the Length of Grapevine Fine Roots: Developmental Anatomy, Tissue-Specific Aquaporin Expression, and Pathways of Water Transport. Plant Physiology 163, 1254–1265. https://doi.org/10.1104/pp.113.221283

Ghanem, M.E., Marrou, H., Sinclair, T.R., 2015. Physiological phenotyping of plants for crop improvement. Trends in Plant Science 20, 139–144. https://doi.org/10.1016/j.tplants.2014.11.006

Gharbi, E., Lutts, S., Dailly, H., Quinet, M., 2018. Comparison between the impacts of two different modes of salicylic acid application on tomato (*Solanum lycopersicum*) responses to salinity. Plant Signaling & Behavior 13, e1469361. https://doi.org/10.1080/15592324.2018.1469361

GIMP development team, 2021. GIMP.

Heymans, A., Couvreur, V., LaRue, T., Paez-Garcia, A., Lobet, G., 2020a. GRANAR, a Computational Tool to Better Understand the Functional Importance of Monocotyledon Root Anatomy. Plant Physiol. 182, 707–720. https://doi.org/10.1104/pp.19.00617

Heymans, A., Couvreur, V., Lobet, G., 2021. Combining cross-section images and modeling tools to create high-resolution root system hydraulic atlases in *ZEA MAYS*. Plant Direct 5. https://doi.org/10.1002/pld3.334

Heymans, A., Couvreur, V., Meunier, F., Lobet, G., 2020b. Hydraulic Viper, a virtual phenotyping pipeline for root hydraulic traits - multiscale approach. Presented at the 9th International Conference on FUNCTIONAL-STRUCTURAL PLANT MODELS, Katrin Kahlen, Tsu-Wei Chen, Andreas Fricke, Hartmut Stützel, FSPM2020: Towards Computable Plants, Institute of Horticultural Production Systems : Hannovre2020, p. 193 p, Hanovre.

Hunter, M.C., Smith, R.G., Schipanski, M.E., Atwood, L.W., Mortensen, D.A., 2017. Agriculture in 2050: Recalibrating Targets for Sustainable Intensification. BioScience 67, 386–391. https://doi.org/10.1093/biosci/bix010

Kim, Y.X., Ranathunge, K., Lee, S., Lee, Y., Lee, D., Sung, J., 2018. Composite Transport Model and Water and Solute Transport across Plant Roots: An Update. Front. Plant Sci. 9, 193. https://doi.org/10.3389/fpls.2018.00193

Kitin, P., Nakaba, S., Hunt, C.G., Lim, S., Funada, R., 2020. Direct fluorescence imaging of lignocellulosic and suberized cell walls in roots and stems. AoB PLANTS 12, plaa032. https://doi.org/10.1093/aobpla/plaa032

Lee, C., 2021. Moneymaker Tomatoes Plant Care & Growing Tips. Horticulture Magazine. URL https://horticulture.co.uk/tomatoes/moneymaker/ (accessed 7.26.22).

Lewis, A.M., Boose, E.R., 1995. E STIMATING VOLUME FLOW RATES THROUGH XYLEM CONDUITS. American Journal of Botany 82, 1112–1116. https://doi.org/10.1002/j.1537-2197.1995.tb11581.x

Li, T., Yang, X., Yu, Y., Si, X., Zhai, X., Zhang, H., Dong, W., Gao, C., Xu, C., 2018. Domestication of wild tomato is accelerated by genome editing. Nat Biotechnol 36, 1160–1163. https://doi.org/10.1038/nbt.4273

Lin, Y.-P., Lu, C.-Y., Lee, C.-R., 2020. The climatic association of population divergence and future extinction risk of Solanum pimpinellifolium. AoB PLANTS 12, plaa012. https://doi.org/10.1093/aobpla/plaa012

Lobell, D.B., Gourdji, S.M., 2012. The Influence of Climate Change on Global Crop Productivity. Plant Physiology 160, 1686–1697. https://doi.org/10.1104/pp.112.208298

Lobet, G., Pagès, L., Draye, X., 2011. A Novel Image-Analysis Toolbox Enabling Quantitative Analysis of Root System Architecture. Plant Physiology 157, 29–39. https://doi.org/10.1104/pp.111.179895

Lux, A., Morita, S., Abe, J., Ito, K., 2005. An Improved Method for Clearing and Staining Free-hand Sections and Whole-mount Samples*. Annals of Botany 96, 989–996. https://doi.org/10.1093/aob/mci266

Lynch, J.P., Chimungu, J.G., Brown, K.M., 2014. Root anatomical phenes associated with water acquisition from drying soil: targets for crop improvement. Journal of Experimental Botany 65, 6155–6166. https://doi.org/10.1093/jxb/eru162

Lynch, J.P., Strock, C.F., Schneider, H.M., Sidhu, J.S., Ajmera, I., Galindo-Castañeda, T., Klein, S.P., Hanlon, M.T., 2021. Root anatomy and soil resource capture. Plant Soil 466, 21–63. https://doi.org/10.1007/s11104-021-05010-y

Maule, A.J., 2008. Plasmodesmata: structure, function and biogenesis. Current Opinion in Plant Biology 11, 680–686. https://doi.org/10.1016/j.pbi.2008.08.002

Meunier, F., Draye, X., Vanderborght, J., Javaux, M., Couvreur, V., 2017. A hybrid analytical-numerical method for solving water flow equations in root hydraulic architectures. Applied Mathematical Modelling 52, 648–663. https://doi.org/10.1016/j.apm.2017.08.011

Meunier, F., Heymans, A., Draye, X., Couvreur, V., Javaux, M., Lobet, G., 2020. MARSHAL, a novel tool for virtual phenotyping of maize root system hydraulic architectures. in silico Plants 2, diz012. https://doi.org/10.1093/insilicoplants/diz012

Miyashima, S., Roszak, P., Sevilem, I., Toyokura, K., Blob, B., Heo, J., Mellor, N., Help-Rinta-Rahko, H., Otero, S., Smet, W., Boekschoten, M., Hooiveld, G., Hashimoto, K., Smetana, O., Siligato, R., Wallner, E.-S., Mähönen, A.P., Kondo, Y., Melnyk, C.W., Greb, T., Nakajima, K., Sozzani, R., Bishopp, A., De Rybel, B., Helariutta, Y., 2019. Mobile PEAR transcription factors integrate positional cues to prime cambial growth. Nature 565, 490–494. https://doi.org/10.1038/s41586-018-0839-y

Moneymaker [WWW Document], 2022. . Tomatofifou. URL https://www.tomatofifou.fr/recherche-variete-2/recherche-multicriteres/moneymaker-detail (accessed 7.26.22).

Naseer, S., Lee, Y., Lapierre, C., Franke, R., Nawrath, C., Geldner, N., 2012. Casparian strip diffusion barrier in *Arabidopsis* is made of a lignin polymer without suberin. Proc. Natl. Acad. Sci. U.S.A. 109, 10101–10106. https://doi.org/10.1073/pnas.1205726109

Nawrath, C., Schreiber, L., Franke, R.B., Geldner, N., Reina-Pinto, J.J., Kunst, L., 2013. Apoplastic Diffusion Barriers in Arabidopsis. The Arabidopsis Book 11, e0167. https://doi.org/10.1199/tab.0167

Pagès, L., Bécel, C., Boukcim, H., Moreau, D., Nguyen, C., Voisin, A.-S., 2014. Calibration and evaluation of ArchiSimple, a simple model of root system architecture. Ecological Modelling 290, 76–84. https://doi.org/10.1016/j.ecolmodel.2013.11.014

Pagès, L., Vercambre, G., Drouet, J.-L., Lecompte, F., Collet, C., Le Bot, J., 2004. Root Typ: a generic model to depict and analyse the root system architecture. Plant and Soil 258, 103–119. https://doi.org/10.1023/B:PLSO.0000016540.47134.03

Passot, S., Couvreur, V., Meunier, F., Draye, X., Javaux, M., Leitner, D., Pagès, L., Schnepf, A., Vanderborght, J., Lobet, G., 2019. Connecting the dots between computational tools to analyse soil–root water relations. Journal of Experimental Botany 70, 2345–2357. https://doi.org/10.1093/jxb/ery361

Pound, M.P., French, A.P., Atkinson, J.A., Wells, D.M., Bennett, M.J., Pridmore, T., 2013. RootNav: Navigating Images of Complex Root Architectures. Plant Physiology 162, 1802–1814. https://doi.org/10.1104/pp.113.221531

Pound, M.P., French, A.P., Wells, D.M., Bennett, M.J., Pridmore, T.P., 2012. CellSeT: Novel Software to Extract and Analyze Structured Networks of Plant Cells from Confocal Images. Plant Cell 24, 1353–1361. https://doi.org/10.1105/tpc.112.096289

R Core Team, 2020. R: A Language and Environment for Statistical Computing. R Foundation for Statistical Computing, Vienna, Austria.

Rezk, A., Abhary, M., Akhkha, A., 2021. Tomato (Solanum lycopersicum L.) Breeding Strategies for Biotic and, in: Al-Khayri, J.M., Jain, S.M., Johnson, D.V. (Eds.), Advances in Plant Breeding Strategies: Vegetable Crops. Springer International Publishing, Cham, pp. 363–405. https://doi.org/10.1007/978-3-030-66961-4_10

Schneider, C.A., Rasband, W.S., Eliceiri, K.W., 2012. NIH Image to ImageJ: 25 years of image analysis. Nat Methods 9, 671–675. https://doi.org/10.1038/nmeth.2089

Schnepf, A., Leitner, D., Landl, M., Lobet, G., Mai, T.H., Morandage, S., Sheng, C., Zörner, M., Vanderborght, J., Vereecken, H., 2017. CRootBox: A structural-functional modelling framework for root systems. bioRxiv 139980. https://doi.org/10.1101/139980

Serra, O., Geldner, N., 2022. The making of suberin. New Phytologist 235, 848–866. https://doi.org/10.1111/nph.18202

Šimůnek, J., Genuchten, M.Th., Šejna, M., 2016. Recent Developments and Applications of the HYDRUS Computer Software Packages. Vadose zone j. 15, 1–25. https://doi.org/10.2136/vzj2016.04.0033

Smetana, O., Mäkilä, R., Lyu, M., Amiryousefi, A., Sánchez Rodríguez, F., Wu, M.-F., Solé-Gil, A., Leal Gavarrón, M., Siligato, R., Miyashima, S., Roszak, P., Blomster, T., Reed, J.W., Broholm, S., Mähönen, A.P., 2019. High levels of auxin signalling define the stem-cell organizer of the vascular cambium. Nature 565, 485–489. https://doi.org/10.1038/s41586-018-0837-0

Steudle, E., 2001a. The cohesion-tension mechanism and the acquisition of water by plant roots. Annu. Rev. Plant. Physiol. Plant. Mol. Biol. 52, 847–875. https://doi.org/10.1146/annurev.arplant.52.1.847

Steudle, E., 2001b. Water uptake by plant roots: an integration of views, in: Gašparíková, O., Čiamporová, M., Mistrík, I., Baluška, F. (Eds.), Recent Advances of Plant Root Structure and Function. Springer Netherlands, Dordrecht, pp. 71–82. https://doi.org/10.1007/978-94-017-2858-4_9

Steudle, E., Oren, R., Schulze, E.-D., 1987. Water Transport in Maize Roots: Measurement of Hydraulic Conductivity, Solute Permeability, and of Reflection Coefficients of Excised Roots Using the Root Pressure Probe. Plant Physiol. 84, 1220–1232. https://doi.org/10.1104/pp.84.4.1220

Steudle, E., Peterson, C.A., 1998. How does water get through roots? Journal of Experimental Botany 49, 775–788. https://doi.org/10.1093/jxb/49.322.775

Strock, C.F., Lynch, J.P., 2020. Root secondary growth: an unexplored component of soil resource acquisition. Annals of Botany 126, 205–218. https://doi.org/10.1093/aob/mcaa068

Strock, C.F., Morrow de la Riva, L., Lynch, J.P., 2018. Reduction in Root Secondary Growth as a Strategy for Phosphorus Acquisition. Plant Physiol. 176, 691–703. https://doi.org/10.1104/pp.17.01583

Strock, C.F., Schneider, H.M., Galindo-Castañeda, T., Hall, B.T., Van Gansbeke, B., Mather, D.E., Roth, M.G., Chilvers, M.I., Guo, X., Brown, K., Lynch, J.P., 2019. Laser ablation tomography for visualization of root colonization by edaphic organisms. Journal of Experimental Botany 70, 5327–5342. https://doi.org/10.1093/jxb/erz271

Taiz, L., Zeiger, E., 2003. Plant Physiology. Sinauer Associates Inc.

Tardieu, F., Draye, X., Javaux, M., 2017. Root Water Uptake and Ideotypes of the Root System: Whole-Plant Controls Matter. Vadose Zone Journal 16, vzj2017.05.0107. https://doi.org/10.2136/vzj2017.05.0107

Tebaldi, C., Lobell, D.B., 2008. Towards probabilistic projections of climate change impacts on global crop yields. Geophys. Res. Lett. 35, L08705. https://doi.org/10.1029/2008GL033423

Tomato “Moneymaker” seeds [WWW Document], 2022. . Thompson-Morgan. URL https://www.thompson-morgan.com/p/tomato-moneymaker/282TM (accessed 7.26.22).

Wasaya, A., Zhang, X., Fang, Q., Yan, Z., 2018. Root Phenotyping for Drought Tolerance: A Review. Agronomy 8, 241. https://doi.org/10.3390/agronomy8110241

Wheeler, T., von Braun, J., 2013. Climate Change Impacts on Global Food Security. Science 341, 508–513. https://doi.org/10.1126/science.1239402

Yang, W., Feng, H., Zhang, X., Zhang, J., Doonan, J.H., Batchelor, W.D., Xiong, L., Yan, J., 2020. Crop Phenomics and High-Throughput Phenotyping: Past Decades, Current Challenges, and Future Perspectives. Molecular Plant 13, 187–214. https://doi.org/10.1016/j.molp.2020.01.008

Yeung, E.C.T., Stasolla, C., Sumner, M.J., Huang, B.Q. (Eds.), 2015. Plant Microtechniques and Protocols. Springer International Publishing, Cham. https://doi.org/10.1007/978-3-319-19944-3

Zelko, I., Lux, A., Sterckeman, T., Martinka, M., Kollárová, K., Lišková, D., 2012. An easy method for cutting and fluorescent staining of thin roots. Annals of Botany 110, 475–478. https://doi.org/10.1093/aob/mcs046

Zhou, X.-R., Schnepf, A., Vanderborght, J., Leitner, D., Lacointe, A., Vereecken, H., Lobet, G., 2020. CPlantBox, a whole-plant modelling framework for the simulation of water- and carbon-related processes. in silico Plants 2, diaa001. https://doi.org/10.1093/insilicoplants/diaa001

Appendices

Appendix 1 : Hoegland nutritive solution

Component	Concentration
KNO_3 [2M]	202g/L
$Ca(NO_3)_2$ x $4H_2O$ [2M]	472g/L
NH_4NO_3 [1M]	80g/L
Minors :	
H_3BO_3	2.86g/L
$MnCl_2$ x $4H_2O$	1.81g/L
$ZnSO_4$ x $7H_2O$	0.22g/L
$CuSO_4$	0.051g/L
H_3MoO_4 x H_2O or	0.09g/L
Na_2MoO_4 x $2H_2O$	0.12g/L
KH_2PO_4 [1M]	136g/L
Iron (Sprint 138 chelate)	15g/L

Appendix 2 : Example of secondary growth cross sections generated with the update of GRANAR

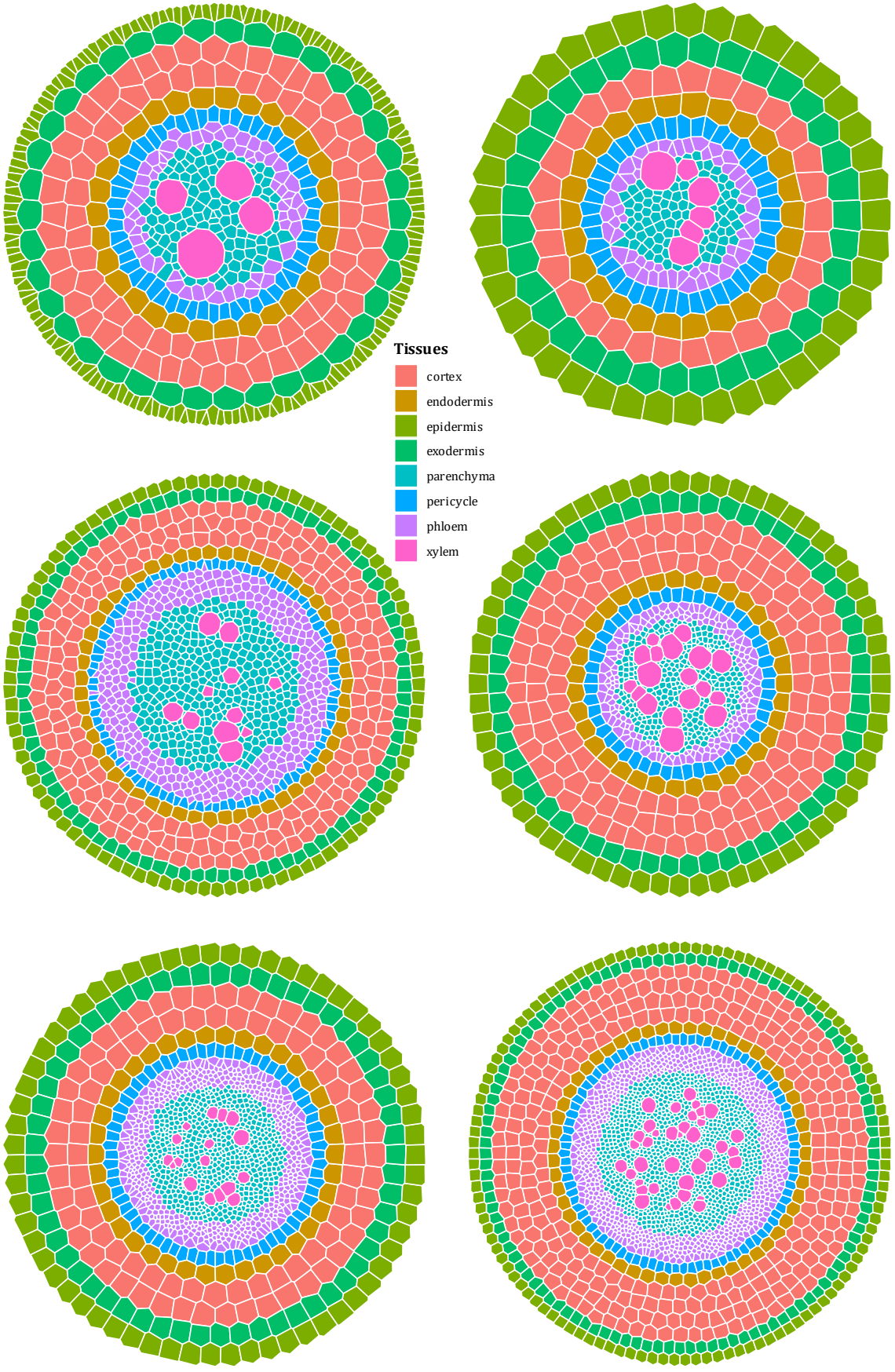

How do root anatomy influences water uptake in tomato?

Updates of protocols and computational tools for the characterization of tomato root anatomy

Marco D'Agostino

Understand the role of plant traits in water uptake is crucial in a climate change context, where droughts that impact crop production are expected to be more frequent and more severe. At the microscopical scale, root anatomy plays a major role in water dynamics. Thus, coupling anatomical traits with architectural traits in phenotyping processes might improve our understanding of water-saving strategies in plants.

However, anatomy is difficult to study with high throughput due to its microscopical scale. New tools and protocols have to be developed to enhance the quality of anatomical modelling, and to integrate anatomy into plant-scale simulations. More specifically, computational tools might help investigate the influence of anatomy on water flow with higher throughput than experimental techniques.

In this master's thesis, we updated GRANAR, a generator of root anatomy, by adding a secondary growth module. For that, we used tomato as model plant. We grew tomato in hydroponics, monitored architectural parameters, and explored tomato root anatomy. Staining techniques were tested and applied, and a protocol for quantifying the root anatomy was built. Tomato root anatomy was characterised, and maturity stages along the tap root were investigated.

With the collected data, we implemented and validated the new R function Pack Xylem, that is integrated in the code of GRANAR and allow the generation of anatomical secondary growth patterns. The virtual cross sections generated with this new module are compatible with a solver of root hydraulic anatomy (MECHA).

The new tools and updated protocols of this work open the gates for new applications, e.g. include local anatomical and hydraulic parameters in simulations of water dynamics at the plant scale.

UNIVERSITÉ CATHOLIQUE DE LOUVAIN
Faculté des bioingénieurs
Croix du Sud, 2 bte L7.05.01, 1348 Louvain-la-Neuve, Belgique | **www.uclouvain.be/agro**